Volume 11, Number 1, 2017

Technical University of Cluj-Napoca
North University Centre of Baia Mare
Faculty of Engineering
Electrical, Electronic and Computer Engineering Department

Volume 11, Number 1, 2017

Carpathian Journal of Electrical Engineering

# Carpathian Journal of Electrical Engineering

ISSN 1843 - 7583

UTPRESS PUBLISHER

TECHNICAL UNIVERSITY
OF CLUJ-NAPOCA

NORTH UNIVERSITY CENTRE OF BAIA MARE
FACULTY of ENGINEERING

ELECTRICAL, ELECTRONIC AND
COMPUTER ENGINEERING DEPARTMENT

# Carpathian Journal of Electrical Engineering

Volume 11, Number 1, 2017

**ISSN 1843 – 7583**
http://cee.ubm.ro/cjee.html

## CONTENTS

# FUZZY LOGIC-BASED AUTOMATIC DOOR CONTROL SYSTEM

Harun **SUMBUL**

*Department of Biomedical Device Technologies, Yesilyurt D.C. Vocational School, Ondokuz Mayis University, 55139, Samsun, Turkey,*

*harun.sumbul@omu.edu.tr*

**Keywords: Automatic door, fuzzy logic, rule bases, control system**

**Abstract***: In this paper, fuzzy logic based an automatic door control system is designed to provide for heat energy savings. The heat energy loss usually occurs in where outomotic doors are used. Designed fuzzy logic system's Input statuses (WS: Walking Speed and DD: Distance Door) and the output status (DOS: Door Opening Speed) is determined. According to these cases, rule base (25 rules) is created; the rules are processed by a fuzzy logic and by appyled to control of an automatic door. An interface program is prepared by using Matlab Graphical User Interface (GUI) programming language and some sample results are checked on Matlab using fuzzy logic toolbox. Designed fuzzy logic controller is tested at different speed cases and the results are plotted. As a result; in this study, we have obtained very good results in control of an automatic door with fuzzy logic. The results of analyses have indicated that the controls performed with fuzzy logic provided heat energy savings, less heat energy loss and reliable, consistent controls and that are feasible to in real.*

## 1. INTRODUCTION

Fuzzy logic is a set of mathematical foundations for knowledge representation based on degrees of membership. Fuzzy logic is use in solving a wide variety of the problems relative to mathematic and engineering. A. Zadeh has developed the mathematical method to produce many complex probing solutions in medical areas [1]. Fuzzy logic has been applied in many areas of engineering and medical. [2-4]. But, it is actually gained a popularity when it was applied to industrial problems [5].

There are a lot of methods to control of automatic doors, such as Field Programmable Gate Array (FPGA) [6], Peripheral Interface Controller (PIC) microcontroller [7], Arduino

[8], Programmable Logic Controller (PLC) [9] etc. Normally; in classical systems, an electronic sensor (Passive Infrared sensor (PIR) sensor) is placed in front of an automatic door and the door opens or closes according to the information from PIR. But the opening speed of the door is fixed and when someone approaches the door, the door starts opening at a constant speed (please attention that detection time is important). However, our used method is considerably remarkable to the control of automatic doors. In our method, the door speed is adjusted to open as required range. People do not wait in front of the door when come. There is less hot air to out from the inside (because of the door don't opened until the end and the door range decreased). Thus saving energy would be provided, *figure 1*.

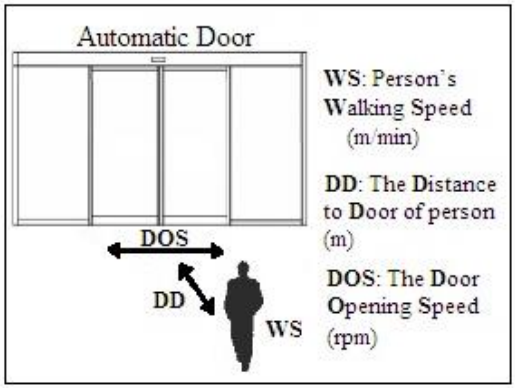


*Fig. 1. Working principle of the designed system.*

## 2. FUZZY SYSTEM CONTROLLER DESIGN

Fuzzy logic controller is recently one of the developing popular methods in control systems. The main idea behind the fuzzy logic controller is to write the rules that operating the controller in heuristic manner, mainly in "*If A Then B* format. Fuzzy systems generally consist of two units; Knowledge-Base and Inference Engine. Knowledge-Base involves real information previously validated. Inference Engine determines answers to the chosen questions by using the information in the database that that composed of rules [10]. The Fuzzy system structure used in this study is given in *figure 2*.

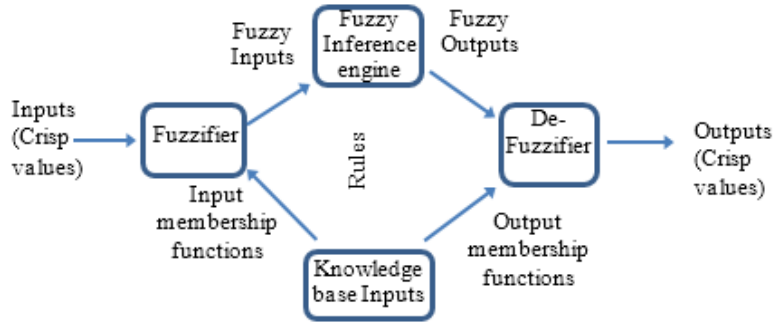


*Fig. 2.The structure of fuzzy logic controller [11].*

Fuzzy System components are described briefly below;

- *Fuzzifier:* This block transforms input information to fuzzy logic data format that can express with linguistic. The blurred variables obtained are called as linguistic.
- *Inference Engine:* This engine generates blurred results by applying the inputs coming from fuzzifier on the knowledge base rules. The most commonly used inference method is mamdani, so in this study it was chosen. Another interface model is the method developed by Takagi and Sugeno and there is no need for defuzzification [12]
- *Knowladge Base:* The knowledge base accumulates the sets of regulations of conclusions that are used in reaching a decision. Most of these systems use IF-THEN programming condition codes to put in practice the knowledge. Knowledge base consists of data base and rule base. The rules may be of the following structure [10]:

*IF (condition (one or more)) THEN (action)*

- *Defuzzifier:* This unit generates nonfuzzy result according to blurred inputs from the fuzzy decision and the actual value that will be used in practice. Decision algorithms can be summarized like; fuzzy [13, 14], Neuro Network [15], Adaptive Neuro fuzzy [16], machine learning [17] etc.

While the fuzzy based controller designing, firstly fuzzy rules were defined as two input variables and one output variable. Figure 3 shows the inputs, the output variables and fuzy control system editor.

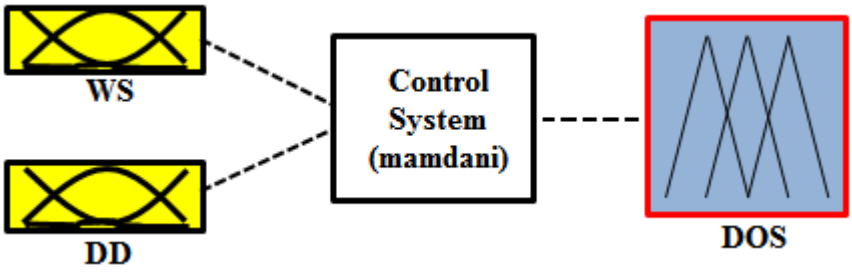


*Fig. 3. Fuzzy Editor.*

### 1.1. Input and Output Variables

In the designed system, two input variables were defined, namely as the person's Walking Speed (WS) and Distance to Door of person (DD). The input variables were sent to the fuzzy expert system, the most appropriate result was found among the defined rules system and state of automatic door was transferred to the output variable as The Door Opening Speed (DOS). Limit values for each fuzzy expression were given below. These parameters were linguisticly classified. Input parameters, output parameters, degree of the membership function and linguistic expressions of designed fuzzy controller were defined as shown in the Table 1.

*1.1.1. Input Variables:*

WS: Person's Walking Speed [0-50 m/min].

WS= VS (Very Slow) – S (Slow) – M (Medium) – F (Fast) – VF (Very Fast)

DD: The Distance to Door of person [0-6 m].

DD= VC (Very Close) – C (Close) – M (Medium) – A (Away) – TA (Too Away)

*1.1.2. Output Variables:*

DOS: The Door Opening Speed [0-500 rpm].

WS= VS (Very Slow) – S (Slow) – M (Medium) – F(Fast) – VF(Very Fast)

Table 1. Input parameters, output parameters, degree of the membership function and linguistic expressions of designed fuzzy controller.

| ***Input variables*** | | ***Output variables*** |
|---|---|---|
| ***WS(m/min)*** | ***DD (m)*** | ***DOS (rpm)*** |
| *VS [0-12,5]* | *VC [0-1,5]* | *VS [0-150]* |
| *S [0-25]* | *C [0-3]* | *S [0-250]* |
| *M [12,5-37,5]* | *M [1,5-4,5]* | *M [125-375]* |
| *F [25-50]* | *A [3-6]* | *F [250-500]* |
| *VF [37,5-50]* | *TA [4,5-6]* | *VF [375-500]* |

## 1.2. Rule Base

The fuzzy controller decides according to the rules contained in the rule base that created with the help of an expert. Essentially, the rules structures consist of statements as "if-then that are intuitive and easy to understand. The rules used in this study are created with the help of an expert. In this study, 25 rules are created by using membership functions. Some rules from prepared rule base are shown in the Table 2.

Table 2. The sets of rule.

| ***Rule No:*** | *Rule structure* | ***Input variables*** | | *Rule structure* | ***Output variables*** |
|---|---|---|---|---|---|
| | *condition* | *WS* | *DD* | *action* | *DOS* |
| *1* | ***if*** | *VS* | *TA* | ***then*** | *VS* |
| *2* | | *VS* | *D* | | *VS* |
| *…* | | *…* | *…* | | *…* |
| *13* | | *M* | *M* | | *M* |
| *14* | | *M* | *C* | | *F* |
| *…* | | *…* | *…* | | *…* |
| *24* | | *VF* | *C* | | *VF* |
| *25* | | *VF* | *VC* | | *VF* |

Membership degrees of the output variable are shown in the Table 3.

Table 3. Rule table for problem.

| | ***DD*** | | | | | |
|---|---|---|---|---|---|---|
| ***WS*** | *TA* | *A* | *M* | *C* | *VC* | |
| *VS* | *VS* | *VS* | *S* | *S* | *M* | |
| *S* | *VS* | *S* | *S* | *M* | *F* | |
| *M* | *S* | *S* | *M* | *F* | *F* | ***DOS*** |
| *F* | *S* | *M* | *F* | *F* | *VF* | |
| *VF* | *M* | *F* | *F* | *VF* | *VF* | |

These rules have been shown as membership functions in *figures 4, 5* and *6*.

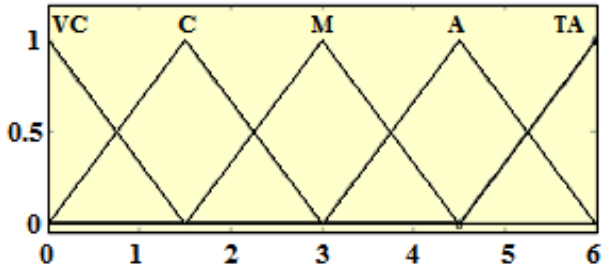


*Fig. 4. Membership functions for DD.*

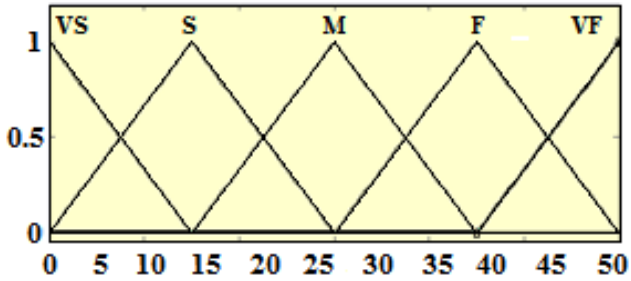


*Fig. 5. Membership functions for WS.*

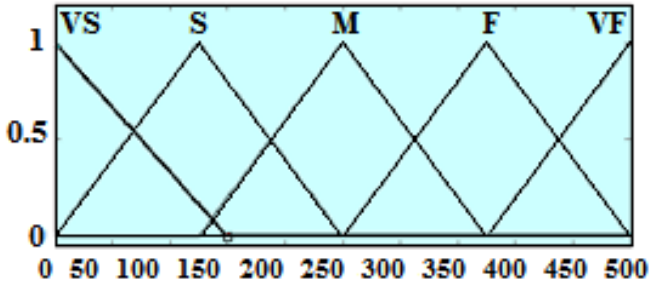


*Fig. 6. Membership functions for DOS.*

### 1.3. Defuzzification Method

In this study, we used the center-of-gravity/area (centroid) defuzzification method, cause it is the most preferred method in litertature. In this method, the output of each membership functions and the corresponding maximum membership value (z*) are calculated by the formula given below (1). $\bar{z}$ is the distance to the centroid of the respective membership functions [5].

$$z^* = \frac{\sum \mu_c(\bar{z}).\bar{z}}{\sum \mu_c(\bar{z})} \tag{1}$$

## 3. RESULTS

The sensors sense the input variables using the above model. After the inputs are fuzzyfied, the output fuzzy function DOS (Door Opening Speed) is obtained by using simple if-else rules and other simple fuzzy set operations. *figure 7* shows the response surface of the input-output relations as determined by Fuzzy Interface Unit (FIU).

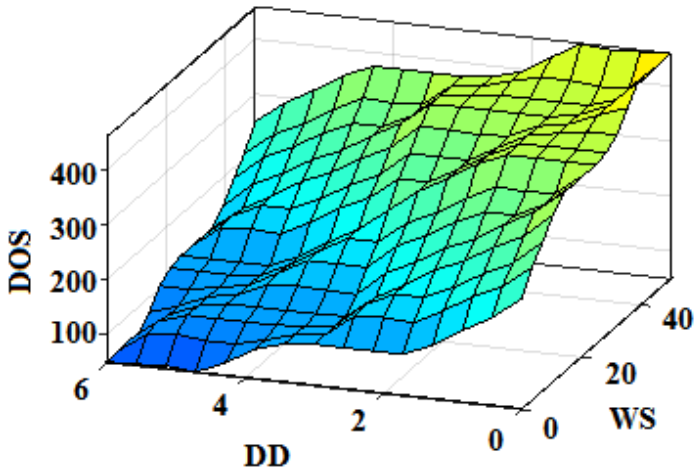


*Fig. 7. Input/output response surface wiever*

Values of each membership functions of fuzzy sets which are formed according to the method are taken weighted average by multiplying each one with its maximum membership degree. The results shows the way the automatic door will response in different conditions. For example, if we take WS= 29.6 and DD= 3.19, DOS which the model output is equivalent to 278 RPM. This is quite convincing and appropriate that as a linguistic ' M (Medium) '. This operation is demonstrated in *figure 8*.

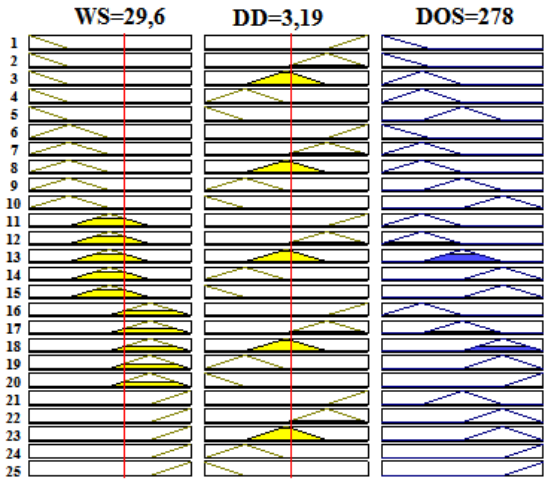


*Fig. 8. Detection of DOS.*

An interface program was developed and prepared by using Matlab Graphical User Interface (GUI) (version R2015b (8.6.0.267246)) programming language to some sample results were checked on Matlab using fuzzy logic toolbox. Then the program calculated degree of DOS as 278 as given in *figure 9*.

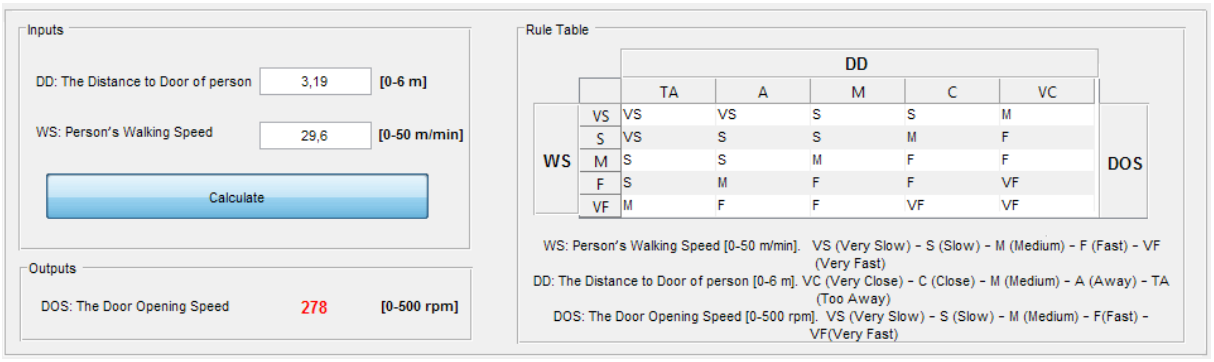


*Fig. 9. Interface program (prepared by using Matlab GUI programming language commands)*

## 4. CONCLUSION

In this paper, an application of fuzzy algorithms in the controller of the automatic door has been investigated.

Opening speed of the automatic door (0-500 rpm) was obtain for different speed of walking (0-50 m/min) and different distance of door (0-6 m) by using a fuzzy logic controller.

In classical systems, the person's distance to the door and the walking speed of the person have no effect on the opening speed of the door. The door do not open until the point in where the person perceives by the sensor and the person may have to wait in front of the door for a while. At that point, the door opens at constant speed. In our control system, as the person's

walking speed increases, the opening speed of the door also increases. Variation of door opening speed according to person's walking speed and distance to door is shown in *figure 10*.

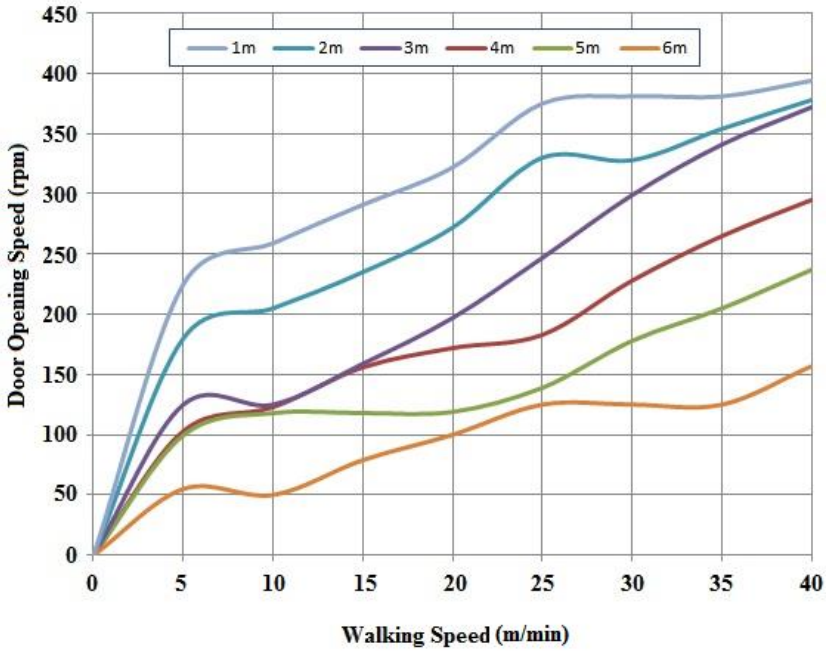


*Fig. 10. Variation of Door opening speed according to the person's walking speed and distance to door.*

## *REFERENCES*

[1] L. A Zadeh, *Outline of a new approach to the analysis of complex systems and decision processes*, IEEE Trans. on Systems, Man and Cybernetics, vol. SMC-3, no. 1, pp. 28-44, 1973.

[2] F. Basciftci, H. Sümbül, *Design an Expert System for Detection of Tuberculosis Disease with Logic Simplification Method*, E-Journal of New World Sciences Academy, vol. 5, no. 3, Seri: 1A, pp. 463-471, 2010.

[3] D. Álvarez-Estévez, V. Moret-Bonillo, *Fuzzy reasoning used to detect apneic events in the sleep apnea-hypopnea syndrome*. Expert Systems with Applications, 36:4: pp. 7778-7785, 2009.

[4] N. Allahverdi, *Design of Fuzzy Expert Systems and Its Applications in Some MedicalAreas*, International Journal of Applied Mathematics, Electronics and Computers, , 2(1), pp. 1–8, 2013.

[5] I. A. Ozkan, I. Saritas, S. Herdem, *The control of magnetic filters by FPGA based fuzzy controller*, Energy Education Science and Technology Part A-Energy Science and Research, vol. 29, no.2, pp. 1093-1102, 2012.

[6] K. M. Al-Ashmouny, H. M. Hamed, A. A. Morsy, *FPGA-based Sleep Apnea Screening Device for Home Monitoring*, Proceedings of the 28th IEEE EMBS Annual International Conference, New York City, USA, 2006.

[7] H. Sümbül, *Mikrodenetleyici Kontrollü Yeni Bir Algılayıcı Tasarımı*, NEWWSA Engineering Sciences, 1A0186, vol. 6, no.2, pp. 672-680, 2011.

[8] H. Sümbül, A. H. Yüzer, *The Measurement of COPD Parameters (VC, RR, and FVC) by using Arduino Embedded System*, Proceedings of 1st International Mediterranean Science and Engineering Congress(IMSEC2016) Çukurova University, Congress Center, October 26-28, pp. 201-207, Adana/Turkey, 2016.

[9] C. Barz, T. Latinovic, Z. Erdei, G. Domide, A. Balan**,** *Practical application with PLC in manipulation of a robotic arm,* Carpathian Journal of Electrical Engineering, vol. 8, no. 1, pp. 78-86, 2014.

[10] F. Basciftci, H. Incekara, *Design of web-based fuzzy input expert system for the analysis of serology laboratory tests*, Journal of Medical Systems, vol. 36, no. 4, pp. 2187-2191, 2012.

[11] R. Kunhimangalam, S. Ovallath, P. K. A. Joseph, *Novel fuzzy expert system for the identification of severity of carpal tunnel syndrome*. BioMed Research International: Article ID 846780, 12 pages, doi:10.1155/2013/846780, 2013.

[12] Z. Erdei, P. Borlan, *Fuzzy logic control,* Carpathian Journal of Electrical Engineering, vol. 5, no. 1, pp. 35-40, 2011.

[13] H. Nazeran, A. Almas, K. Behbehani, E. Lucas, *A fuzzy inference system for detection of obstructive sleep apnea*, Proceedings of the 23rd Annual International Conference of the IEEE Engineering in Medicine and Biology Society, vol. 2, pp. 1645-1648. doi: 10.1109/IEMBS.2001.1020530, 2001.

[14] K. M. Al-Ashmouny, A. A. Morsy and S. F. Loza, *Sleep apnea detection and classification using fuzzy logic: clinical evaluation*, IEEE Engineering in Medicine and Biology, Proceedings of 27th Annual Conference, Shanghai, pp. 6132-6135. doi: 10.1109/IEMBS.2005.1615893, 2005.

[15] J. Y. Tian, J. Q Liu, *Apnea detection based on time delay neural network*, IEEE Engineering in Medicine and Biology, Proceedings of 27th Annual Conference, Shanghai, pp. 2571-2574. doi: 10.1109/IEMBS.2005.1616994, 2005.

[16] F. Z. Abdel-Mageed, F. E. Z. Abou Chadi, H. M. Salah, S. F. Loza, *Detection of sleep apnea events using analysis of thoraco-abdominal excursion signals and adaptive neuro-fuzzy inference system (ANFIS)*, Proceedings of 29th National Radio Science Conference (NRSC), Cairo, pp. 691-698. doi: 10.1109/NRSC.2012.6208584, 2012.

[17] A. Q. Javaid, C. M. Noble, R. Rosenberget, M. A. Weitnauer, *Towards Sleep Apnea Screening with an Under-the-Mattress IR-UWB Radar Using Machine Learning*, Proceedings of 14th International Conference on Machine Learning and Applications (ICMLA), Miami, FL, pp. 837-842, doi: 10.1109/ICMLA.2015.79, 2015.

# IMAGE STEGANOGRAPHY TAILORED TO OBJECTS CONTOURS

Ovidiu **COSMA**
*Technical University of Cluj-Napoca, North University Center of Baia Mare*
*ovidiu.cosma@yahoo.com*

**Keywords: image steganography, LSB substitution**

**Abstract***: This article proposes a steganography method that uses all three components of an image in the RGB color space to store secret data. The order in which the image pixels are processed is not given by their position within the image, but by their visual significance. In order to ensure the greatest possible embedding capacity, the image container is traversed in several passes, each expanding its capacity.*

## 1. INTRODUCTION

Steganography is a technique for data security that hides the secret information into a container that will unveil its true content only to the consignee. Text, audio, photos, and video files can be used as secret data containers. The image steganography techniques operate in the spatial domain or in the frequency domain. The secret data is called payload and the image with hidden data inside is known as stego image. Among the applications of steganography are: secret communication, copyright control, feature tagging and video-audio synchronization.

The key features of the steganography techniques are: robustness strength and capacity. Robustness refers to the resistance the payload against the processing operations applied to the container. In the case of image steganography, these operations could be geometric transformations, contrast, brightness or saturation adjustment, histogram correction, compression, cropping, blurring or detail enhancement, noise addition, etc. Strength indicates how difficult it is for anyone to guess that there is something else hidden inside the container. Capacity is the amount of hidden data that fits inside the container.

The art of breaking steganography is called steganalysis. For increasing the strength of steganography, the data embedding technique must preserve the perceptual quality as well as the statistical properties of the container.

## 2. IMAGE STEGANOGRAPHY

Digital images are composed of pixels, usually represented by 32 bits integers. Each pixel color is composed of four components of eight bits. The first component represents the pixel opacity and the following three represent the intensities of the Red Green Blue (RGB) components that simulate the pixel color.

One of the oldest digital image steganography techniques uses one or more of the least significant bits (LSBs) from the pixel RGB components for storing the secret data. The amount of secret data stored in each pixel, determines the visual quality of the stego image. The distortions caused by changing the pixel values are more visible in image areas without large amounts of details. As a consequence, if large payloads are needed, the uniform use of all image pixels is not recommended.

A technique of increasing the payload known as Bit Plane Complexity Segmentation (BPCS) is presented in [1]. The image is divided into 8 x 8 pixel blocks that are classified by complexity. Only the high complexity blocks will be used for placing the secret data.
Another steganography technique based on BPCS is presented in [2]. It differs from BPCS in the way the complexities of the image blocks are deterimned. A steganography technique that uses gray level images is presented in [3]. In [4] is presented a method that embeds secret data by altering the differences between pixels. It takes into account the complexities of the image regions to determine the proper amount of secret data to be stored in each of the pixels. A steganography technique appropriate for compressed images is presented in [5]. It is demonstrated by the authors to have high embedding capacity, and to allow for the perfect reconstruction of the original image.

In general, the spatial steganography techniques have the advantage of simplicity and high capacity, but they have the disadvantage of low robustness and strength. Several transform domain techniques have been proposed, for increasing the strength of image steganography. They apply an initial transformation in which the image is converted from the spatial domain to the frequency domain. Then the embedding of secret data is performed by altering some of the transform coefficients. There are several techniques to choose the coefficients that will keep the secret data. In [6] is presented a technique designed for JPEG compressed images [7]. The secret data is embedded by altering the LSB of the quantized Discrete Cosine Transform (DCT) coefficients that are different from 0, 1 and -1. Another steganographic technique for JPEG iamges is presented in [8]. It is different by the fact that the coefficients that will store the secret data are randomly selected. Another technique that

uses a genetic algorithm for selecting the best DCT coefficients to store the secret data is presented in [9]. The advantage of this method is the fact that it resists to almost all known steganalysis methods.

## 3. STEGANOGRAPHY DETECTION

The art of detecting steganography is called steganalysis. The only disadvantage of LSB steganography lays the fact that it is easily detectable. The LSB steganography principle stands on the assumption that the LSB of image pixels are random, and they can be replaced without creating suspicion. In [10] it is shown that this assumption is not correct, and in fact the pixels LSBs are correlated. Those correlations can be easily obserserved if only the LSB of each pixel is represented as a binary image. As a consequence the hidden data can be visually detected, because it disrupts those correlations.

In reality, such correlations do not occur in any image. In fact they rarely occur in the case of older images that are converted in one of the new formats for digital images. A statistical steganalysis method has been proposed in [10], for overcoming the limitations of the visual method. This method, known as the chi-square attack calculates a probability for the presence of hidden data depending on the length of the analyzed sample.

## 4. THE PROPOSED STEGANOGRAPHIC METHOD

The proposed method differs from the original LSB substitution method, by the fact that the secret data embedding process can involve one or mode passes through the whole image, depending on the amount of secret data. All the three components (RGB) of the image are used. The last significant bits (LSBs) of the RGB components are not used, because there are numerous steganalysis methods that verify their distribution. The next three bits may be used for secret data embedding. The image pixels are processed in an order determined by a contour detection filter. The secret data is passed through an encryption algorithm, which ensures an extra level of security while increasing the strength of the method.

The operations of the proposed method are presented in *figure 1*. The first block shifts the values of the RGB components of each image pixel with four positions to the right. Thus the last four bits of each component are lost. This step ensures that the following operations will not take into account the stego data, and will be accurately reproduced at decoding. The second block applies a contour detection filter. In principle, any such filter may be used. The Sobel filter [11] was used in the experiments. This processing produces for each pixel a value that reflects the importance of the contour on which the pixel stands.

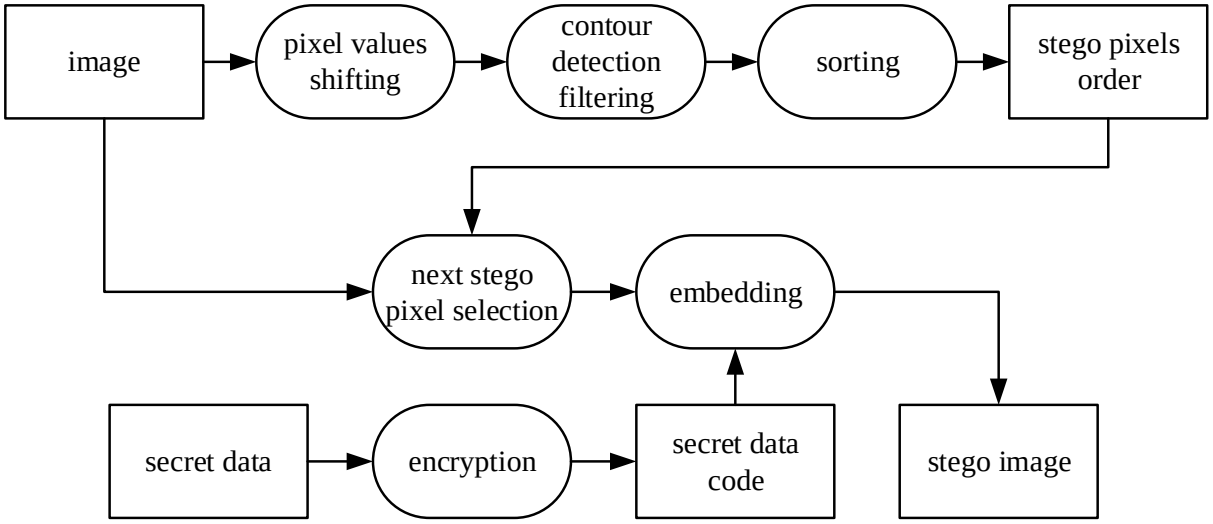


*Fig. 1. Operation of the proposed method*

For pixels in uniform regions, free of color variations, the value 0 is obtained. These pixels can not be altered too much in the embedding operation, as there is a danger that changes will become visible. Pixels on the contours of objects can be modified to a greater extent without causing noticeable distortions. The next block performs the sorting of image pixels by the values obtained in the filtering step. This step determines the order in which image pixels will be processed in the secret data embedding operation. The process begins with the pixels on the most important contours and ends with the pixels in areas lacking details. The last bit of the RGB components will not be used in the embedding process. At the first pass, the second of the LSBs will be used for embedding the secret data. Since these bits are relatively unimportant, all image pixels can be used in this pass, without the danger of creating noticeable artefacts. Thus, at the first pass, the capacity of the container can be calculated as follows:

```
imageWidth * imageHeight * 3 [bits]
```

This initial capacity can be expanded if needed by the following passes. In case of massive secret data, such as digital images, the embedding operation may require several passes. In each of the following passes, the pixels of the image will be processed in the order given by the sorting block, starting with those on the most important contours.

At the second pass, the third of the LSBs will be used. Experiments have shown that no detectable distortions can occur in this pass, but for extra security, the pixels in areas lacking details will not be used for embedding the secret data. Thus, the second pass ends when pixels are reached for which the value calculated by the contour detection filtering block is below a certain threshold (*t1*). The optimal value of *t1* depends on the type of contour filter used. The amount by which container capacity can be expanded in the second pass depends not only on the size of the image, but also on its content. For example, for a completely white picture, there are no available pixels in the second pass.

If the secret data embedding process does not end in the second pass, then the operation continues with a new pass in which the fourth of the LSBs will be used. At this stage, the pixels that will be changed should be chosen with even greater caution. As in the previous pass, the process starts with the pixels that are on the most important contours, and ends when the value calculated by the contour detection filtering block is below a certain threshold (*t2*), where *t2 > t1*. As with *t1*, the optimal value of *t2* depends on the type of contour filter used.

The differences between the proposed method and the other known methods are as follows: the image container is processed in several passes, it does not use image segmentation based on complexity, the image pixels are sorted based on an edge detection filter, the last bit of the three RGB color components is left unchanged.

## 5. EXPERIMENTAL RESULTS

The digital image container which was used for presenting the results of the proposed method is shown in *figure 2*. It has a resolution of 512 x 512 pixels and occupies 512 x 512 x 3 / 1024 = 768 kB of memory. This container was filled up to full capacity with random data. Thus, in the first pass, all pixels of the image were used, resulting a capacity of 96 kB. This capacity was expanded in the second and third passes with 59 kB and 29 kB respectively, resulting a total capacity of 184 kB, that is more than enough to keep inside a payload of 9 JPEG images of good quality and having the same size as the container image. The capacity of the image container is 184 / 768 *100 ≈ 24%. Of all the staganography techniques presented in paragraph 2, BPCS [1], [2] has the highest embedding capacity (approximately 50%).

*Fig. 2. Original image*

*Figures 3* and *4* show the stego pixels used in the second and in the third pass. Even if the entire capacity of the container has been used, there are no apparent differences between the original and the stego images. The PNG format has been used to save the stego image because it is a lossless format. The size of the stego image file is 440 KB.

One of the most powerful steganography techniques is the genetic algorithm approach [9]. It is known to defeat all the steganalysis techniques. The proposed method has good strength, combined with larger capacity. Even if the entire capacity of the container is used, the chi-square attack [10] does not reveal anything, because the last bit of the pixels components was not used in the embedding process. *Figure 5* presents the results of the chi-square attack applied on the stego image filled up to full capacity with random data.

*Fig. 3. Stego pixels used in the second pass*

*Fig. 4. Stego pixels used in the third pass*

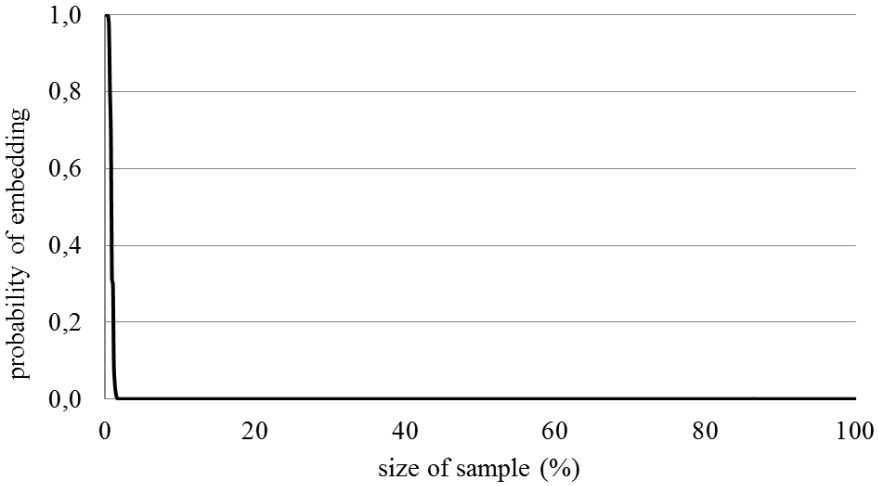


*Fig. 5. The result of the chi-square attack, applied on the stego image*

## 5. CONCLUSIONS

The image steganography method presented in this article uses all three components of an image in the RGB color space to store the payload, and processes the image in multiple passes, to ensure a hingh embedding capacity. The embedding capacity of the proposed method is not constant at a given image resolution. It depends on the amount of details in the image container.

For increasing the strength of the method, at each pass the image pixels are processed in an order given by their visual significance. The method is not vulnerable to the chi-square attack, because the last bit of the three color components (RBG) is not used in the embedding process.

The proposed method is not robust. Any processing performed on the image container could destroy its payload. But only watermarking needs robustness, steganography does not.

## *REFERENCES*

[1] M. Niimi, H. Noda, E. Kawaguchi, *A Steganography Based on Region Segmentation by Using Complexity Measure*, Trans. of IEICE, Vol. J81-D-II, No. 6, 1998.

[2] H. Hioki, *A data embedding method using BPCS principle with new complexity measures*, Proceedings of Pacific Rim Workshop on Digital Steganography, 2002.

[3] V.M. Potdar, E. Chang, *Gray level modification steganography for secret communication*, Proc. of 2nd IEEE International Conference on Industrial Informatics, pp. 223-228, 2004.

[4] D. Wu, W.H. Tsai, *A steganographic method for images by pixel value differencing*, Pattern Recognit. Lett. 24, pp.1613-1626, 2003.

[5] H.C. Wu, H.C. Wang, C.S. Tsai, C.M. Wang, *Reversible image steganographic scheme via*

*predictive coding*, Displays, no.31, pp. 31-43, 2010.

[6] D. Upham, *Jsteg*, http://zooid.org/ paul/crypto/jsteg/ (accessed: 2017-05).

[7] Gregory K. Wallace, *The JPEG still picture compression standard*, Communications of the ACM, vol. 34(4), pp.30-44, April 1991.

[8] A. Latham, *JPHIDE*, http://linux01.gwdg.de/ alatham/stego.html (accessed: 2017-05).

[9] A. Milani, A. Mohammad, A. Varasteh, *A New Genetic Algorithm Approach for Secure JPEG Steganography*, IEEE International Conference on Engineering of Intelligent Systems, 2006.

[10] A. Westfeld, A. Pfitzmann, *Attacks on Steganographic Systems Breaking the Steganographic Utilities EzStego, Jsteg, Steganos, and S-Toolsand Some Lessons Learned*, https://users.ece.cmu.edu/ adrian/487-s06/westfeldpfitzmann- ihw99.pdf (accessed: 2017-05).

[11] Irwin Sobel, *History and definition of the so-called Sobel Operator*, https://www.researchgate.net/publication/239398674_An_Isotropic_3_3_Image_Gradient_Operator (accessed 2017-05).

# STRUCTURAL MONITORING OF WIND TURBINES USING SENSORS CONNECTED VIA UTP CABLE

Dumitru **SPERMEZAN**, Mircea I. **BUZDUGAN**, Horia **BALAN**
*Technical University of Cluj-Napoca*
dumitruspermezan@yahoo.com

**Keywords: vibrometer, vibrations monitoring, piezoelectric transducer, acquisition board**

**Abstract:** Unpredicted faults that may occur at the wind generators elements affect their economic operation. A promising approach that avoids these faults is the real-time vibrations monitoring. Data measured by the sensors can be transmitted to a monitoring station using wireless techniques, or optical fiber, or UTP cable. The last possibility is the cheapest, but it permits connecting the monitoring station at a limited distance with respect to the monitored turbine. The paper presents the components of the monitoring system and the experimental results related to the monitored wind turbine.

## 1. INTRODUCTION

Amongst the mechanical components of wind turbines, the biggest percent of faults occurs in the gear box. In [1], is shown that the principal reason of these faults comes from the ball bearings, which determine the lack of reliability of the gear boxes and consequently the longest time of stagnation of the wind turbines.

For the monitoring and the diagnosis, the measurement and the analysis of the vibration spectrum is used [2]. The vibration spectrum offers information regarding the incipient faults and contributes to the formation of a reference signature, which may be used in further monitoring processes. The vibration spectrum of an equipment containing faulty ball bearings has one or more frequencies generated by the faulty element. Most often and especially when a fault occurs in an incipient stage, the vibrations determined by the faulty balls will be reduced in amplitude, compared to the vibrations of the moving components, like shafts, cogwheels, etc. The frequencies denoting the faults cannot be noticed using the time or the spectrum analysis of the vibrations.

The processing techniques of such a signal have several limitations. For instance, some faults cannot be diagnosed using the fast Fourier transform (FFT), if the load value is reduced or if the fault is not too severe. Thus, in these situations it is preferable to use other techniques, like: the Wavelet transform, the Cepstrum analysis or the Hilbert transform.

The monitoring method, based on wavelet transform presents a high sensitivity, a short detection time and can be easily applied for online monitoring. This method is based on the principle of the restoration of all the signals in sets of signals of different dimensions and amplitudes, but constants in form.

In the last years, the Wavelet transform techniques have been used to analyze the nonstationary vibrations, generated by faults occurring on the external periphery of the ball bearings [3]. In [4] the properties of the bandwidth of the vibrations are analyzed and in order to identify the ball bearings faults, the Wavelet transform is applied. These studies demonstrated that the time-frequency analysis of the vibrations signals, generated by ball bearings, provides a large amount of information related to the conditioning of the component elements of the ball bearings. In [5] the identification of the faults in a gear box is presented, the approach being performed using the amplitude and the frequency demodulation of the current of an induction motor which is driving a gear box. The discrete Wavelet transform is applied in order to cancel the unwanted noises from the current signal and uses a certain level of the frequency spectrum, to detect the possible faults in the gear box. This is somehow a singular study in the literature, because the majority of the studies state that the faults in the gear box cannot be detected by analyzing the current signals of the generator connected thereto.

Since the modern wind electric generators, capable to develop powers of megawatts are available on the market, efficient maintenance and fault detection methods are needed. The online monitoring systems offer a new prospect on maintenance and fault prevention strategies. Using new monitoring systems, the faults can be detected in incipient stages, even before being visible or noticed from the acoustic stand point. Therefore, preventive maintenance measures can be used, before the fault would degenerate in a secondary fault. Thus, the maintenance overall cost is significantly reduced. Using these systems, the maintenance plan can be extended to larger periods of time, avoiding accordingly premature alteration of the functional components. Replacing the main components can be an extremely expansive and time consuming process. At the same time an online monitoring system may offer certain advantages:

- prevention of secondary and/or major faults;
- reduction of the maintenance costs by applying the conditioned maintenance;
- remote survey and diagnosis;
- detailed information related to the performance of the equipment and to its vibrations.

## 2. VIBRATIONS MONITORING

The structure of a vibrations transducer has as a significant feature the fact that the sensitive element provides at its output a mechanical value: force or displacement. In order to obtain an electrical signal, able to be processed by an adapter, an intermediary converter, that converts a mechanical value to an electrical value is needed. The separation between the element sensitive to vibrations and the intermediary converter has a functional character, but from the constructive standpoint, the two parts, usually form a single unit. The most often the intermediary converter is a piezoelectric one, determining an electric polarization noticeable between the two opposite surfaces of the crystal perpendicular to the faces submitted to a mechanical force. The polarization value is proportional to the applied force and it changes its direction with the direction of the force as well. The piezoelectric effect is explained by the deformation of the crystalline grid, which determines the deterioration of the electrical equilibrium established between the grid atoms.

The functional properties of a piezoelectric converter may be deduced if the mechanical parameters describing its operation are set equivalent to the electrical parameters. This can be done using the electro-mechanical analogies, based on the formal identity of the differential equations that describe a mechanical system and an electrical circuit. Starting from these analogies and taking into account the operation of a piezoelectric crystal, the equivalent electric schematic may be drawn, *fig. 1*.

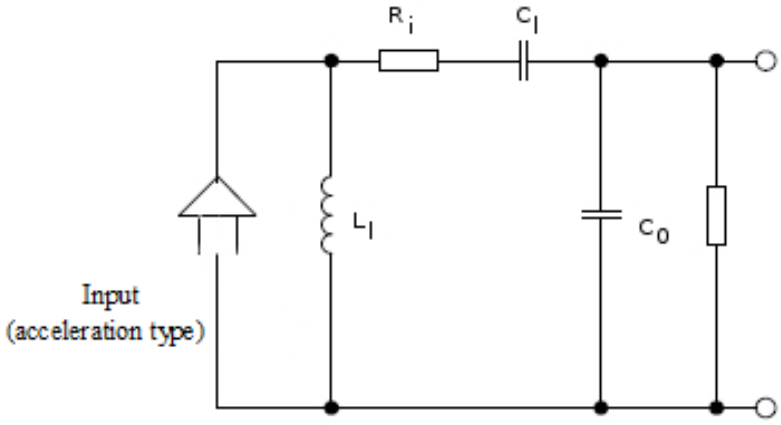


*Fig. 1. Equivalent schematic of the piezoelectric converter.*

The equivalent circuit of a converter, cable connected, is presented in *fig. 2*. The piezoelectric element acts like a capacity $C_a$ parallel connected with a high value equivalent parallel resistance $R_a$ (EPR). The piezoelectric element can be considered as a charge source $Q_a$, or a voltage source $V_a$. As one can notice from *fig. 2*, the voltage $V_a$ is dependent of the cable capacity. Thus, the calibration factor for determining the voltage sensitivity of the

convertor, must take into account the connection cable. If different cables than those specified are used, correction coefficients depending on the capacity of the new cable must be introduced, or a new voltage sensitivity must be considered.

An important parameter for achieving a proper operation of the converters is the transverse sensitivity, determined versus the applied acceleration under square angles with respect to the main axis. It is expressed in percent versus the load sensitivity or the voltage, measured with respect to the main direction. It must be mentioned that the maximum sensitivity is not obtained versus the main direction of the piezoelectric crystal, in which, maximum and minimum directions of sensitivity exist. Usually, the minimum sensitivity direction is labelled on the device housing. For an ideal piezoelectric material, the transverse sensitivity is zero, but in reality, due to the fabrication imperfections, it differs from zero, reaching three percent of the main sensitivity. The dependency of the transverse sensitivity versus frequency is depicted in the catalog sheet of the producer.

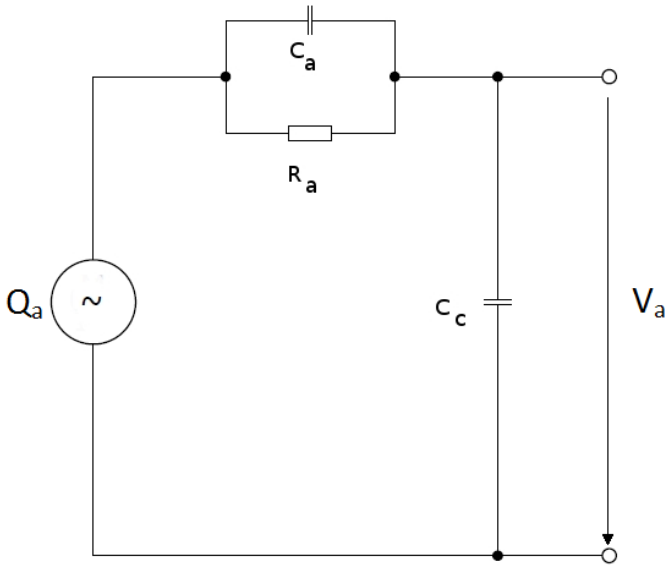


*Fig. 2. Equivalent schematic of the voltage generator.*

A special attention must be paid to the measurement of the chokes and of the transients, since important errors may occur, like for instance the displacement error in relation to zero, or the ringing error.

The displacement error in relation to zero is due to the phase nonlinearities generated in the amplifier by the low frequency components of the real signal. These distortions don't affect the average value, but they can influence the accurate determination of the peak value. In order to maintain these errors in certain imposed limits, it is compulsory that the inferior limit of the preamplifier be lower than a value inverse proportional to a choke or to the period of a transient. It is also recommended the use of acceleration type sensitive elements, because the integration of a single choke in order to obtain velocity or displacement, introduces phase nonlinearities.

The displacement in relation to zero may be produced by the converter itself, especially when high level chokes are applied, determining that only a fraction of the charge stored in the piezoelectric element to be transmitted for measurement.

The ringing error occurs when the frequency spectrum of the choke contains frequency components close to the mechanical resonance frequency. In order to make errors less than an imposed value, a preamplifier and a low pass filter in the input are needed.

If the piezoelectric converters are used beyond the maximum temperature specified for piezoelectric materials, the piezoelectric elements depolarize themselves, determining a permanent loss of the charge and consequently the lowering of the sensitivity. The explanation of this phenomenon consists in the modification of the electric permittivity of the material versus temperature. An analysis regarding this phenomenon shows that the Rochelle salt can't be accepted as a piezoelectric sensitive material, due to its instable properties versus the temperature. There are also several varieties of barium titanate having a different behavior versus temperature. Conversely, the lead zirconate-titanate has practically the same stability as the quartz. One solution in increasing time stability of the sensitivity versus time and temperature consists in the artificial aging.

## 3. ANALOG TO DIGITAL CONVERSION

Monitoring the operating conditions of an electric machine may estimate the moment of the maintenance process. A periodic monitoring of the operation parameters of the equipment, using analysis vibration techniques, makes possible the detection of the problems associated to the wind electric generators. Consequently, the possible issues can be previewed and detected fast enough, in order to draw a repair planning, instead of a preventive maintenance. Measuring vibrations in different locations of the wind electric generator and tracking their intensity in time, represent a reliable and efficient approach, indicating the weary state of an equipment and its time involution. Using a vibrometer permits the visualization of the measurement results, directly in situ. Modern vibrometers have the possibility to store the measurement results in the internal memory of the vibrometer in different equipment, USB connected thereto. The saved results of the measurements can be downloaded later through a communication port and a RS 232 serial interface or a USB interface, provided at the new generation of vibrometers.

Connecting the vibrometer to a PC and using one of the available communication ports, permit also to download and save the data. In order to use a USB communication port, a dedicated driver, delivered by the producer, is compulsory to be installed. For the serial communication port, RS232, the special drivers are not needed. The data being stored in the PC, the user can export them in special application, able to view and compare them with other previous similar data.

Each producer of measurement equipment has developed applications, which are working together with the equipment in order to extract and export data. These applications are most often closed source, meaning a compiled ready version, unmodifiable by the user for his special needs. The closed source applications save data in specific files. Thus, the user is forced to use the applications provided by the manufacturer.

Some vibrometers have the ability to transmit the measured and amplified signals to a special analogic port in order to be processed by further equipment. This signal can be taken over by an acquisition board, that converts an analog signal into a digital one.

Such an acquisition board is 232M1A0CT [6]. The acquisition board, *fig. 3,* has eight analog inputs and ten digital inputs. The analog inputs are unipolar and admit voltages between 0 and 10 Vd.c. The board is supplied by a direct current voltage, in the range from 7.5 V to 24 V and a direct current of 50 mA.

The communication with the monitoring system is made via a RS232 interface. The transmission is made in duplex synchronous mode, each transmitted or received word containing eight data bits, one parity bit and one start/stop bit.

The interface RS232 permits the connection of the monitoring system at a maximum distance of 15 m.

Communication through the RS232 port uses three wires: the first for transmitting data, the second for receiving data and the third for grounding. Between the transmitting and receiving wires and the ground, one can measure values between -8 V and +12 V, respectively +8 V and -12 V. The more complex applications impose a confirmation method of the transmitted data, for preventing the buffer overflow and for verifying the equipment status as well.

In order to control the flux of data between the two equipment the standard words Request to Send-RTS and Clear to Send-CTS are used. The words Data Set Ready-DSR and Data Terminal Ready-DTR are the most used words to call and to answer to the interrogations.

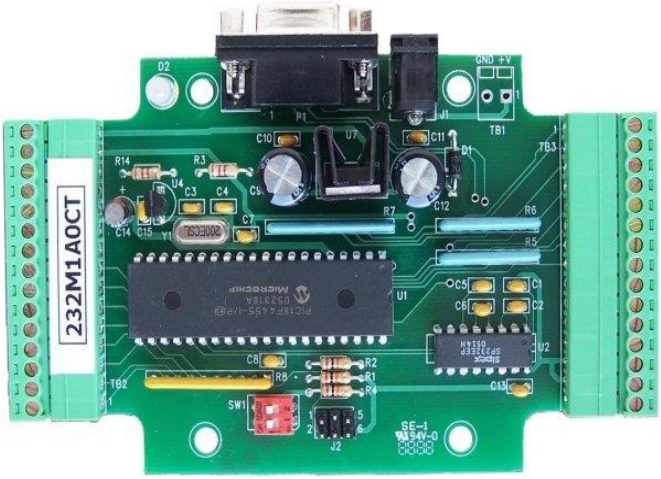


*Fig. 3. The acquisition board is 232M1A0CT*

## 4. REMOTE DATA TRANSMITTING TECHNIQUES

If the monitoring station is situated at a distance of more than 15 m related to the measuring point, the following methods of data transmission can be used:

- Wireless data transmission;
- Optical fiber data transmission;
- UTP cable data transmission.

Wireless grids represent networks of interconnected equipment by radio waves, infrared waves and other wireless methods. In the last years, the wireless techniques have greatly developed, being a reliable and simple alternative solution to cable links. Wireless connections become more and more popular, while they solve problems that appear in the case of large grids of several devices. Modern technologies are able to interconnect equipment situated at small to large distances.

A Wireless Local Area Network- WLAN represents a communication system implemented like an extension or an alternative to a cabled LAN, in a building or a campus, combining connectivity at high speed, providing the mobility of the users in a more simplified configuration. Obvious advantages, like mobility, flexibility, simple commissioning, reduced maintenance costs and scalability have imposed WLAN as a more often used solution.

There are two types of wireless transmitting/receiving equipment:

- Base Stations;
- Subscriber Units.

The base stations antennas have usually a wide angle, ranging from 60 degrees to 360 degrees capable to assure the connectivity of all the customers in a certain area. The base stations can be connected to an optical fiber cable network or radio relays.

The antennas of the subscriber units have a much narrower angle and therefore they have to be oriented towards the base station.

Optical fibers are used on large scale in telecommunications, permitting long distance transmissions having higher band widths than other media communication. Through optical fibers, a signal is transmitted with reduced losses, being immune to electromagnetic interference as well. Consequently, they are used instead of the electrical cables, in lighting technique and images transmission, permitting the visualization in narrow areas. Some of special designed optical fibers are used in several applications, including sensors and laser applications. The waveform in the optical fibers is directed through the core of the fiber using the total reflection, which leads to a waveguide behavior of the optical fiber. The fibers that support several propagation or transverse modes are the so called multimode fibers – MMF, and the fibers that support only one propagation mode are the so called single mode – SMF. The multimode fibers have in general a larger diameter of the core and are used in short distance

communications and in applications in which a higher transfer of power is needed. The single mode fibers are used in communications at distances over 550 m.

The junctioning of the optical fibers is a more complex process than the junctioning of the conventional cables. The extremities of two optical fibers cables must be properly prior prepared and afterwards welded using an electric arc technique. Special connectors, suitable for flexible connections, are used.

Data transmission via optical fiber is performed using both types of fiber, both having the same diameter of 0.12 mm.

The multimode fiber has a larger core diameter, usually of 62.5 μm, but there are also optical fibers having the core diameter of 50 μm, used together with LED lighting sources, having wavelengths of 850 nm and 1300 nm for low speed connections and with laser sources, having wavelengths of 850 nm and 1300 nm for high speed connections of several gigabytes per second.

The single mode fiber has a thinner core, of only 9 μm, and the waveform is transmitted in one flux. It is used together with laser sources having wavelengths between 1300 nm and 1550 nm.

In order to connect the acquisition board with the monitoring station via optical fiber, a pair of RS232 and RS485 converters is needed. The connection between the acquisition board and the monitoring station could be achieved with lower costs using a UTP cable. This connection is possible only for distances of maximum 15 m, without ancillary equipment, with a maximum baud-rate of 115200 bauds/s. If the baud-rate is lower, the equipment can be connected at a longer distance. For instance, for a baud rate of 9600 bauds/s the possible connection distance becomes 150 m.

In order to maintain a high value baud-rate, a current loop converter can be used, *fig. 4*. The converter performs the conversion between the RS232 serial interface to the current loop of 20 mA or 60 mA. This device need an external supply source as well.

Two such converters are needed. The first is needed for transmitting signals from the RS232 port of the acquisition board and the second for receiving data at the RS232 port of the acquisition board.


*Fig. 4. RS232 to current loop converter.*

## 5. EXPERIMENTAL SETUP

The experimental setup using a UTP cable connection is composed of the following elements:

- Piezoelectric transducer Dytran 3100B 6221;
- Sound and vibrations analyzer Svan 912 AE;
- Oscilloscope Fluke 196;
- Acquisition board 232M1A0CT;
- Calibration generator vibrometer RTF.

The piezoelectric transducer is connected via a coax cable to the input port of the sound and vibrations analyzer, Svan 912AE. The analyzer is provided with a converter, that converts the electrical charge to a voltage, which permits the charge measurement. The converter can be also connected to analog measurement instruments via a BNC connector. This feature is used in the experimental setup to connect an oscilloscope. *fig 5,* represents a picture of the experimental setup.

*Fig. 5. Experimental setup, simulating the wind turbines vibrations monitoring.*

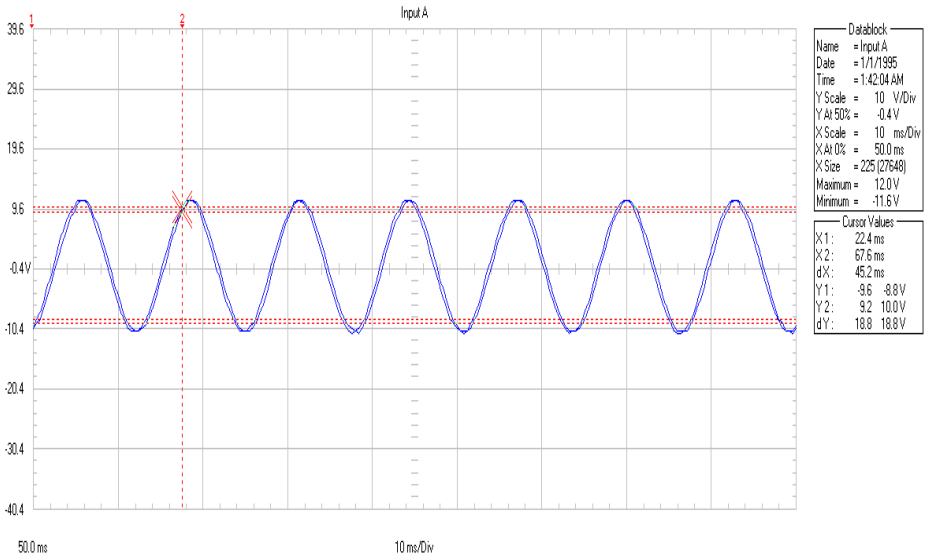


*Fig. 6. The sinusoidal vibration oscillogram.*

The piezoelectric transducer is mounted on the vibrations source using a magnetic pad, consisting of a permanent magnet assuring the transmission of the vibration generated by the undistorted source.

The vibrations source is provided with a control element which is able to modify the vibrations amplitude. Using the vibrations source, the normal operation of the wind generator is simulated.

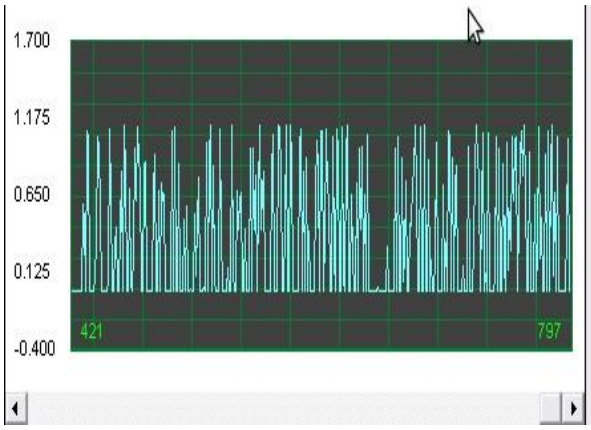


*Fig. 7. Amplitude versus time spectrum at the output of the acquisition board.*

Both the oscillogram of the sinusoidal vibration, *fig. 6*, and the amplitude versus time spectrum, *fig. 7*, highlight a normal operation of the wind generator. Notice that the output of the acquisition board has only a positive component, due to the fact that the input of the acquisition board admits only positive voltages, ranged between 0 Vd.c. to 10 Vd.c.

In order to simulate the faulty situation, the vibration generator generates also chokes, *fig. 8*, presenting non-sinusoidal vibrations. *Fig. 9* depicts situation in which the chokes determine the monitoring system to signal a faulty situation.

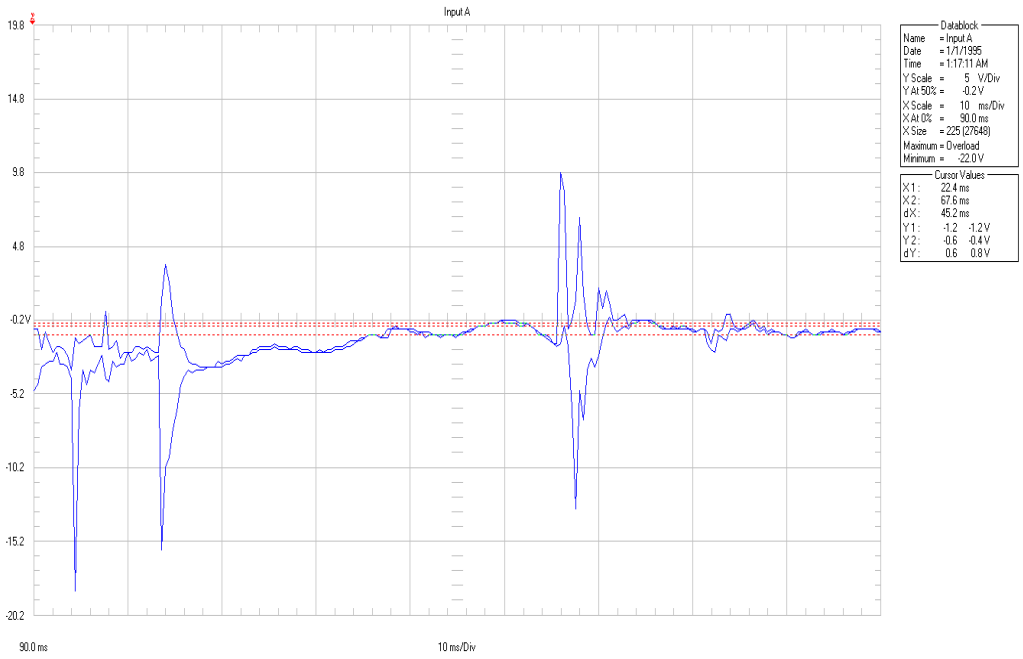


*Fig. 8. The non-sinusoidal vibration oscillogram.*

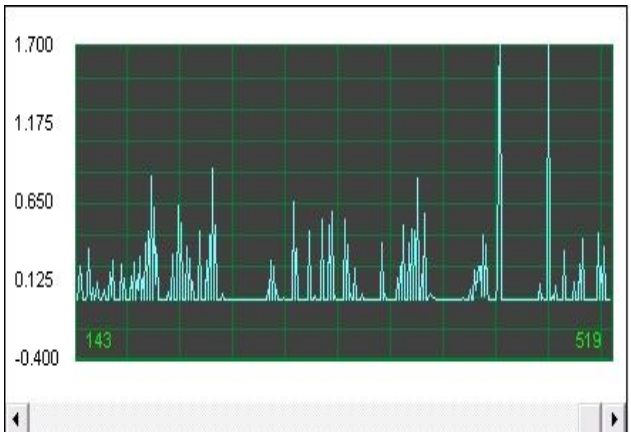


*Fig. 9. The amplitude-time spectrum at the output of the acquisition board in case of a fault.*

## 6. CONCLUSIONS

In order to simulate a faulty operation, a variable vibrations source is used, the control circuit having the possibility to determine the generation of chokes, that simulate the operation of the wind turbine in case of fault.

The experimental results depicted in *figs. 6-9* highlight the role of the acquisition board in the monitoring equipment. The measured values can be saved in CVS type files, a format that doesn't need special drivers for being open and read.

Using an acquisition board capable monitoring more piezoelectric transducers mounted on the main elements of a wind generator, exhaustive information, during the operation time of the wind generator can be obtained. Therefore, the faults of these elements may be detected in incipient stages. Consequently, a repair planning can be drawn, more effective than applying simple preventive maintenance measures. Consequently, major faults that can make the wind generator inoperable could be avoided.

## *REFERENCES*

[1] W. Musial, S. Butterfield, B. McNiff, *Improving Wind Turbine Gearbox Reliability*, European Wind Energy Conference ,Milan, Italy, May 7–10, 2007.

[2] http://www.bksv.com

[3] Paul D, *Detection of change in process using wavelets*, Proc. IEEE-SP Int. Symp. Time-Frecquency and Time Scale Analysis, 174-177, 1994.

[4] Ladd M.D and Wilson G.R., *Proportional bandwidth properties of fault indicating tones in a ball bearing system*, the 28-th Asilomar Conf. Signals, Systems and Computer, 45-49, 1994.

[5] A.R. Mohanty et al., *Fault detection in a multistage gearbox by demodulation of motor current waveform*, IEEE Trans. Industrial Electronics, vol. 53, no.4, pp. 1285-1297, August 2006.

[6] *** www. Integrity Instruments Inc.com

# A METHOD FOR DENOISING IMAGE CONTOURS

Ovidiu **COSMA**
*Technical University of Cluj-Napoca, North University Center of Baia Mare*
*ovidiu.cosma@yahoo.com*

**Keywords: edge detection, noise removal**

**Abstract***: The edge detection techniques have to compromise between sensitivity and noise. In order for the main contours to be uninterrupted, the level of sensitivity has to be raised, which however has the negative effect of producing a multitude of insignificant contours (noise). This article proposes a method of removing this noise, which acts directly on the binary representation of the image contours.*

## 1. INTRODUCTION

Contour detection is a fundamental technique of image processing. Edges and contours play a key role in the human visual system and underpin computer vision applications, such as robot guidance, automatic inspection, process control, and medical applications. Contours play a key role in the perception of images. It is often possible to understand the content of an image that has been reduced to a few basic lines. Consequently, we can conclude that a major part of information in an image lays in objects contours.

Despite the importance of the subject, at present there is no known technique of tracing perfect contours. This is due to the fact that there is a need to compromise between the following two complementary features: thin and uninterrupted contour lines and the absence of false contours (no noise).

## 2. METHODS OF EDGE DETECTION

The contours in an image are made up of pixels for which brightness changes steeply after a certain orientation. The first contour detection methods are based on gradients, which are calculated using first-order derivatives in horizontal and vertical directions [1, 2]. If we

look at a digital image as a function of two variables $f(x,y)$, then the gradient vector is defined according to relation (1), and the gradient magnitude is defined in relation (2).

$$\nabla f(x,y) = \begin{bmatrix} \frac{\partial f}{\partial x}(x,y) \\ \frac{\partial f}{\partial y}(x,y) \end{bmatrix} \tag{1}$$

$$|\nabla f(x,y)| = \sqrt{(\frac{\partial f}{\partial x}(x,y))^2 + (\frac{\partial f}{\partial y}(x,y))^2} \tag{2}$$

The points on the contours are those for which the magnitude of the gradient exceeds a certain threshold. A simple binarization operation can be applied for tracing the contours. The following two filters, known as Roberts filters [1, 2], can be used to estimate the gradient. They determine diagonal contours, but are not very sensitive to orientation. Because they are as small as possible, they can detect the finest contours.

$$H_1^R = \begin{bmatrix} 0 & 1 \\ -1 & 0 \end{bmatrix}, \qquad H_2^R = \begin{bmatrix} -1 & 0 \\ 0 & 1 \end{bmatrix} \tag{3}$$

Any contouring technique has to deal with noise-related issues, because they can be mistakenly interpreted as edges. For this reason, it is preferable to apply a smoothing filter before edge detection [1, 2]. Any smoothing filter would solve this problem, but it is preferable one that does not affect too much the edges. The Gaussian filter defined in relation (4) is frequently used because it is configurable by standard deviation $\sigma$, which determines the width of the bell.

$$G(x,y) = \frac{1}{2\pi\sigma^2} e^{-\frac{x^2+y^2}{2\sigma^2}} \tag{4}$$

This smoothing step may be omitted if the filters that are used calculate the average values of the gradient. The next two filters (Sobel) calculate at each step the gradient average on 3 lines, respectively on 3 columns [1-3]. *Figure 1.b* shows the contours of the image in *figure 1.a*, drawn by applying the Sobel filters, followed by a thresholding operation.

$$H_x^S = \begin{bmatrix} -1 & 0 & 1 \\ -2 & 0 & 2 \\ -1 & 0 & 1 \end{bmatrix}, \qquad H_x^S = \begin{bmatrix} -1 & -2 & -1 \\ 0 & 0 & 0 \\ 1 & 2 & 1 \end{bmatrix} \tag{5}$$

The main problem of all the gradient based techniques is the fact that they rely on the first-order derivative, which is nonzero in ramps. For this reason, they draw relatively thick contours and artificial thinning techniques are required. To solve the problem, edge detection techniques based on the second order derivative were developed [1, 2]. They draw thinner contours, but they have the disadvantage of doubling roof edges.

The Laplace operator for an image $f(x,y)$ is obtained by summing the second order derivatives calculated in the horizontal and vertical directions.

$$\nabla^2 f(x,y) = \frac{\partial^2 f}{\partial x^2}(x,y) + \frac{\partial^2 f}{\partial y^2}(x,y) \tag{6}$$

*Figure 2.a* was generated using the Laplace operator followed by thresholding. The Laplacian filters can detect fine edges, but they have a high sensitivity to noise. As a result, a pre-smoothing operation is required. For efficiency, the two operations (smoothening and edge detection) can be combined into a single one using a Laplacian of Gaussian (LoG) filter that can be calculated based on the following relation:

$$LoG(x,y) = -\frac{1}{\pi\sigma^2}\left[1 - \frac{x^2+y^2}{2\sigma^2}\right] e^{-\frac{x^2+y^2}{2\sigma^2}} \tag{7}$$

*Figures 2.b* and *2.c* were generated using the LoG filter, with a standard deviation $\sigma$ of 0.8 and 1.4 respectively.

An optimized contour detecting method known as the Canny operator is proposed in [4]. The proposed method comprises the following steps:

1. Apply a Gaussian smoothing filter to the original image, for noise reduction.
2. Use the Sobel filters to determine both gradient magnitude and gradient orientation.
3. Apply a contour-thinning algorithm that reduces all contours to one pixel thickness. In the case of thick contours, only the pixel with maximum gradient magnitude in the direction of the gradient orientation remains. All other pixels will be removed from the contour.
4. To avoid discontinuous contours, a hysteresis thresholding algorithm is proposed. This algorithm uses two thresholds. In the first step, a higher threshold is used, based on which the pixels belonging to contours are set. In the second step, a lower threshold is used, based on which other pixels are added to the contours, provided they are connected to the pixels selected in the first step.

The contour image in *figure 1.c* was generated by applying the Canny operator on the image in *figure 1.a.*

*a.) Original image* *b.) Sobel filter* *c.) Canny operator*

*Fig. 1. Original image and contour images*

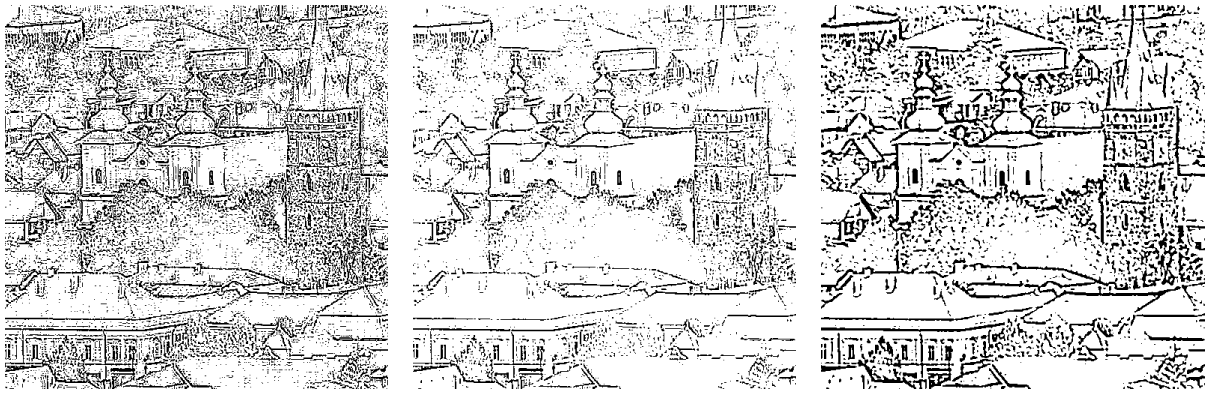

*a.) Laplacian filter* *b.) LoG filter, $\sigma = 0.8$* *c.) LoG filter, $\sigma = 1.4$*

*Fig. 2. Image contours*

## 3. RECENT RESULTS

A Laplacian of B-spline operator for edge detecting is proposed in [6]. The authors claim that the new operator outperforms the Canny and the LoG operators in the case of noisy images. In [7] is presented a new method for detecting the boundaries of homogenous regions. The method is based on gradient intensity and texture variations. The wavelet transform is used for calculating a texture representation. A method based on non-linear filtering for structure preserving noise reduction and edge / corner detection is presented in [8]. A multi resolution edge detection technique is proposed in [9]. For increasing accuracy, the algorithm performs edge pattern analysis. A parallel implementation that runs in real-time is presented. In [10] is presenred a new contour detection algorithm that is based on quantum entropy. The efficiency of the method is demonstrated using different examples. The performance is evaluated using the peak-signal-to-noise ratio. An edge detecting method based on fractional Fourier transformation is presented in [11]. The authors show that the proposed method performs better than classical methods in terms of resilience to noise. A method of contour detection based on the Canny operator enhanced with an ant colony optimization algorithm

is presented in [12]. A new contour detection method for color images is presented in [13]. The method is based on the vector angle between adjacent pixels. An edge detection method based on a logarithmic image processing model is presented in [14]. The author claims that the proposed method performs better than the classical methods in the presence of noise. A new contour detection method is proposed in [15]. The method is based on gradient calculation, followed by a frequency domain filtering step.

A multiresolution contour detection method is proposed in [16]. The method is based on Bayesian denoising and inhibition of the surroundings. The gradient is calculated at different resolutions then the edges are denoised. In the surrounding inhibition step, the edges that represent texture are recognized and suppressed. A technique based on local and global analysis is proposed in [17]. The contour detection is performed by integrating the local edges detected by filtering with a global saliency map. A histogram difference function is presented, for estimating the probability of the pixels to belong to contours. A multi-scale morphological edge detection algorithm for noisy images is presented in [18]. The key features of the algorithm are robustness and accuracy. An evaluation of the linear methods for image contour detection is presented in [19]. The methods are evaluated on basis of sampling errors, output noise level, and computational complexity.

## 4. THE PROPOSED METHOD

Of all the filters for edge detection, the Laplacian filter has the most promising results, but they are shadowed by the high level of noise. The only way to reduce noise is to raise the binarization threshold, but this operation may cause important contours to be interrupted. The LoG filter introduces an additional parameter that can adjust the noise level. This is the standard deviation $\sigma$ that controls the width of the Gaussian filter that performs the initial smoothing operation. But unfortunately, the initial filtering does not completely solve the problem. A large $\sigma$ also affects the thickness of contour lines.

The proposed method is different from the existing ones by the fact that it acts at the end (after the LoG filter and the thresholding operation), on the binary contour image. The method operation is presented in *figure 3*.

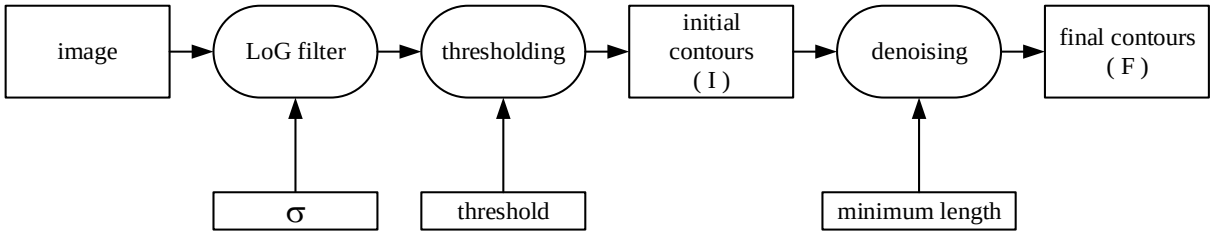


*Fig. 3. Operation of the proposed method*

The denoising block performs the following operations:

1. All the pixels of the final contours image ( F ) are initialized with white.
2. The initial contours image ( I ) is traversed along lines and columns. For each black pixel encountered, the following processing is performed:
   2.1. Initialize a list with the position of the pixel,
   2.2. Change pixel color to white,
   2.3. Add to the list all the black neighbors of the pixel, and their black neighbors, and the black neighbors of their neighbours, etc. Change the color of all pixels added to the list in white. The eight neighbors of the pixel on line y and column x are shown in *figure 4*.
   2.4. If the number of items in the list exceeds a certain threshold, then the color of all the pixels in image F that are located in the positions indicated by the list elements will be changed to black.

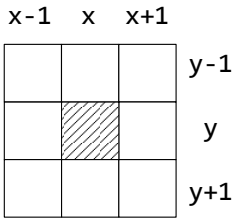


*Fig. 4. A pixel neighbors locations*

## 5. EXPERIMENTAL RESULTS

The image in *figure 1.a* was used for demonstrating the performance of the method. The images obtained after applying the LoG filter for different values of the standard deviation $\sigma$ are shown in *figure 5*. To avoid the interruption of important contours, a relatively small threshold was chosen. This adds a lot of noise in the countours. The result of applying the contour cleaning algorithm is shown in *figure 6*.

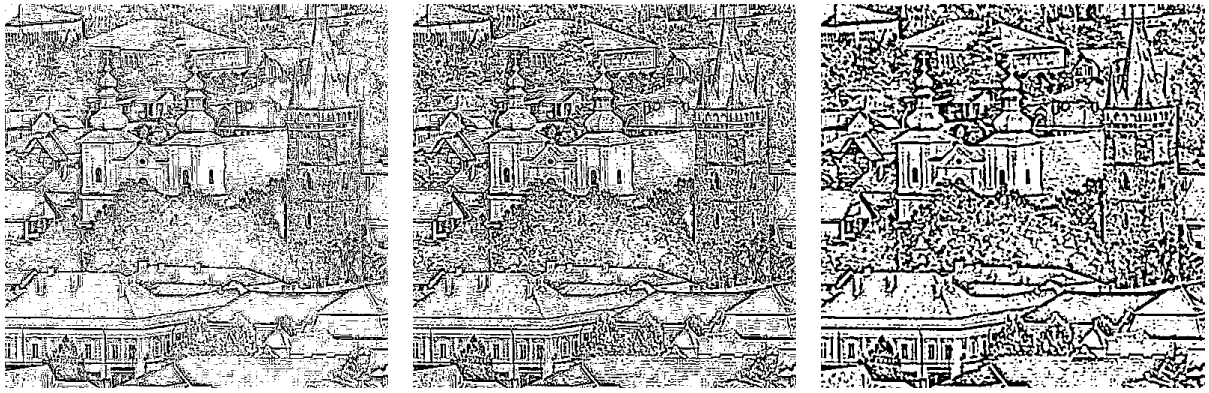

*a.)* $\sigma = 0.6$ *b.)* $\sigma = 0.8$ *c.)* $\sigma = 1.4$

*Fig. 5. LoG filter contours*

*a.)* $\sigma = 0.6$ *b.)* $\sigma = 0.8$ *c.)* $\sigma = 1.4$

*Fig. 6. Cleaned LoG filter contours*

For verifying the properties of the method, it was applied on a set of "standard images, which are commonly used in literature. The test images are presented in *figure 7*. They were taken from [20]. The contours of these images were drawn using the Sobel and Roberts filters, the Canny operator and the proposed method. The results are presented in *figures 8.1* and *8.2*.

*a.) Cameraman* *b.) Jetplane* *c.) Pirate* *d.) Blonde woman* *e.) Peppers*

*Fig. 7. Set of test images*

*a.) Sobel filter* *b.) Roberts filter* *c.) Canny operator* *d.) Proposed method*

*Fig. 8.1. Comparison of the results*

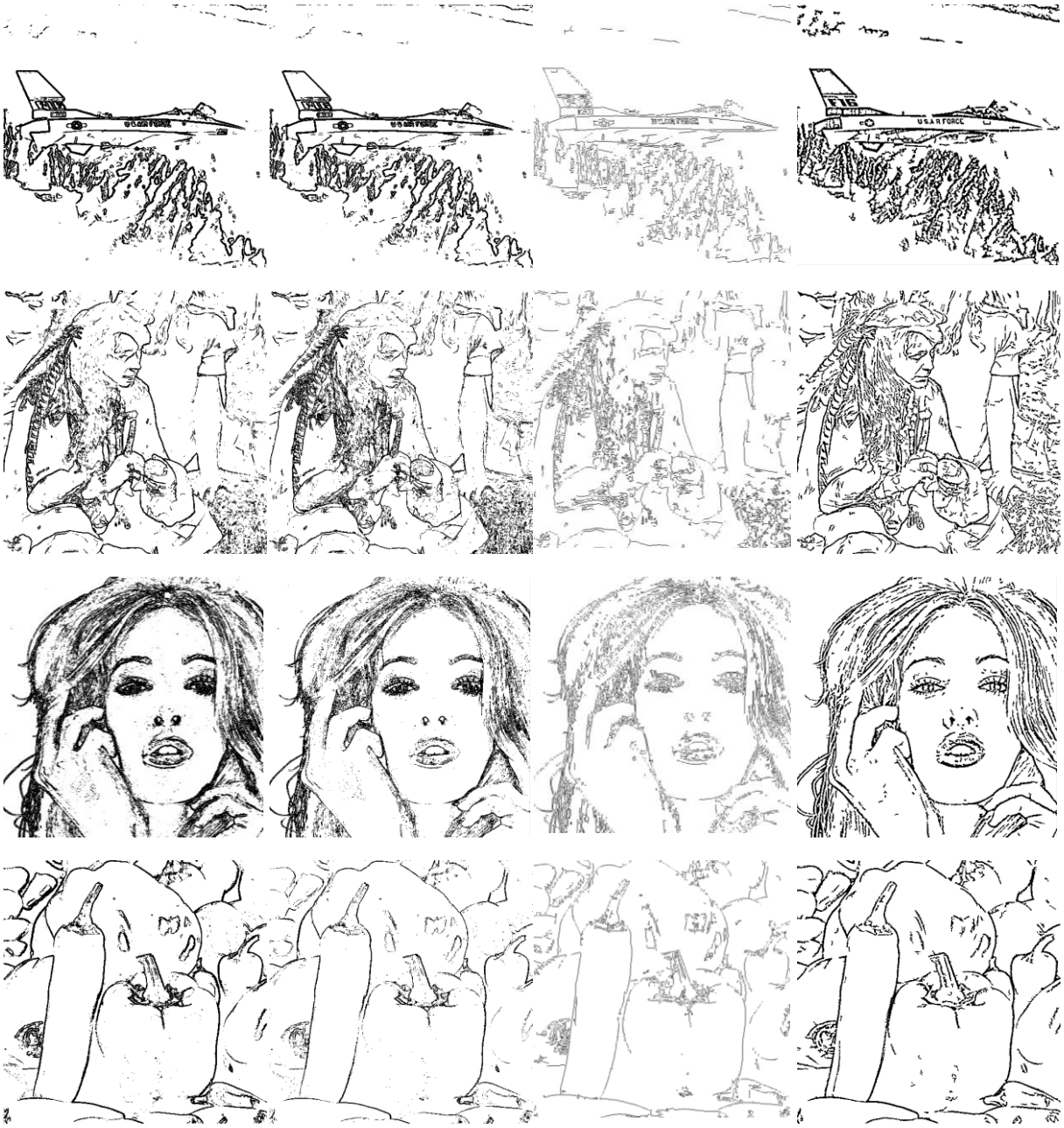

*a.) Sobel filter* *b.) Roberts filter* *c.) Canny operator* *d.) Proposed method*

*Fig. 8.2. Comparison of the results*

## 6. CONCLUSIONS

The method presented in this paper can be used to eliminate noise from contours generated with the LoG filter, adding an additional optimization parameter: minimum length (the minimum number of adjacent black pixels). This allows lowering the binarization threshold, to avoid interrupting important contours. The proposed algorithm is relatively simple and acts directly on the binary representation of the image contours. The contours

obtained in this way are clean and firm. They are visually superior to those obtained using classical techniques.

## *REFERENCES*


[1] Wilhelm J. Burger, Mark J. Burge, *Principles of Digital Image Processing*, Springer, 2013.

[2] Rafael C. Gonzalez, Richard E. Woods, *Digital Image Processing*, Prentice-Hall, 2002.

[3] Irwin Sobel, *History and definition of the so-called Sobel Operator*, https://www.researchgate.net/publication/239398674_An_Isotropic_3_3_Image_Gradient_Operator, (accessed 2017-05).

[4] John Canny, *A Computational Approach to Edge Detection*, IEEE Transactions on Pattern Analysis and Machine Intelligence, Vol. 8, Issue 6, November 1986, pp. 679 – 698.

[5] D. Marr; E. Hildreth, *Theory of Edge Detection*, Proceedings of the Royal Society of London, Series B, Biological Sciences, Vol. 207, No. 1167, pp. 187-217, 1980.

[6] Dongqing Xu, Xiuyou Wang, Gang Sun, Huaimin Li, *Towards a novel image denoising method with edge-preserving sparse representation based on laplacian of B-spline edge-detection*, Multimedia Tools and Applications, 2015.

[7] Nasser Chaji, Hassan Ghassemian, *Texture-Gradient-Based Contour Detection*, Journal on Applied Signal Processing, pp. 1–8, 2006.

[8] Stephen M. Smith, J. Michael Brady, *SUSAN—A New Approach to Low Level Image Processing*, International Journal of Computer Vision Vol. 23, Issue 1, pp. 45–78, 1997.

[9] Bo Jiang, *Real-time multi-resolution edge detection with pattern analysis on graphics processing unit*, Journal of Real-Time Image Processing, pp. 1-29, 2014.

[10] S. Abdel-Khalek, Gamil Abdel-Azim, Z. A. Abo-Eleneen, A.-S. F. Obada, *New approach to image edge detection based on quantum entropy*, Journal of Russian Laser Research, Volume 37, Number 2, March, 2016.

[11] Sanjay Kumar, Rajiv Saxena, Kulbir Singh1, *Fractional Fourier Transform and Fractional-Order Calculus-Based Image Edge Detection*, Circuits, Systems, and Signal Processing, Vol. 36 Issue 4, April, pp. 1493-1513, 2017.

[12] P. Hinduja, K. Suresh, B. Ravi Kiran, *Edge Detection on an Image Using Ant Colony Optimization*, Proceedings of the Second International Conference on Computer and Communication Technologies, pp. 593-599, September 2015.

[13] Young-Hyun Baek, Oh-Sung Byun, Sung-Ryong Moon, Deok-Soo Baek, *Edge Detection in Digital Image Using Variable Template Operator*, International Conference on Knowledge-Based and Intelligent Information and Engineering Systems, pp. 195-200, 2005.

[14] Guang Deng, *Differentiation-Based Edge Detection Using the Logarithmic Image Processing Model*, Journal of Mathematical Imaging and Vision Vol. 8, pp. 161–180, 1998.

[15] Qu ZhiGuo, Gao YingHui, Wang Ping, Wang Peng, Tan XianSi, Shen ZhenKang, *Contour detection improved by frequency domain filtering of gradient image*, Science China Information Sciences, Volume 57, Issue 1, January, pp. 1–11, 2014.

[16] Giuseppe Papari, Patrizio Campisi, Nicolai Petkov, Alessandro Neri, *A Biologically Motivated*

*Multiresolution Approach to Contour Detection*, Journal on Advances in Signal Processing, Vol. 2007.

[17] Hong Cheng, Lin Chen, *A Holistic Approach for Efficient Contour Detection*, Journal of computer science and technology, Vol. 29, Issue 6, pp.1038-1047, November 2014.

[18] Tang Zhengjun, Song Jianshe, *A multi-scale morphological approach to SAR image edge detection*, Journal of electronics, Vol. 17, No. 3, July 2000.

[19] M. Yu. Khomyakov, *Comparative Evaluation of Linear Edge Detection Methods,* Pattern Recognition and Image Analysis, Vol. 22, Issue 2, June, pp. 291–302, 2012.

[20] http://www.imageprocessingplace.com/root_files_V3/image_databases.htm, (accessed 2017-07).

# TESTING SOLUTIONS OF THE PROTECTION SYSTEMS PROVIDED WITH DELAY MAXIMUM CURRENT RELAYS

Horia **BALAN**, Mircea I. **BUZDUGAN**, Ionut **IANCAU**, Liviu **NEAMT**
*Technical University of Cluj-Napoca, Romania*
*horia.balan@eps.utcluj.ro*

**Keywords: power system protection, current relays**

**Abstract**: *Relay protection is one of the main forms of automation control of electro energy systems, having as primary aims fault detection and disconnection of the faulty element in order to avoid the extent of damages and the as fast as possible recovery to the normal operation regime for the rest of the system. Faults that occur in the electro energy system can be classified considering on one hand their causes and on the other their types, but in the vast majority of cases the causes of the faults are combined. Further, considering their nature, faults are classified in faults due to the insulation's damage, in faults due to the destruction of the integrity of the circuits and faults determined by interruptions. With respect to their nature, faults are short circuits, earthing faults and phases interruptions. At the same time, considering their type, faults are divided in transversal and longitudinal ones. The paper presents a testing solution of the delayed maximal current relays using a T3000 ISA Test measuring equipment.*

## 1. INTRODUCTION

A very important issue of the a. c. power grids consists in defining the command, control and protection strategy, meant to assure the normal, safe and stabile operation of the system.

There are several elements which must be considered in the choice of the protection system. The design and the choice of a protection system implies the knowledge of the faults that may appear in electric grids. From the point of view of the effects, immediate or delayed in time, these faults may be of a greater or lesser intensity. Current relays represent the primary protection in the distribution systems. The development of electronic devices, replaced the old electromechanical technology, used in the first generations of protective relays, with the static

technology. However, static relays present several drawbacks, since analog circuits are very sensitive to electromagnetic interference. On the other hand, the magnitudes of the voltage and the currents are limited in analog circuits, affecting the relay sensitivity.

Embedding a microprocessor in the architecture of a relay, which emulate the function and the logic of a relay dates from the early eighties.

Digital relays represent sophisticated equipment, having multiple uses and having the possibility of recording signals during the fault, monitoring and communicating with other relays in the grid. Digital relays use dedicated microprocessors for processing digital signals, being therefore more rapid, and efficient, but maintaining in the same time their economic advantage.

Most of situations, it is impossible to investigate the above mentioned features in a real case of a system, due to different economic, functional of security impediments. Therefore, several approaches and equipment have been developed, in order to overcome these deficiencies: e.g. real time digital simulators (RTDS), reversible real time digital simulators and software packages for modeling protective relays [1].

Digital models of the protective relays offer an economic and reliable alternative in the analysis of relays performance and of the protection systems. At the same time, they permit a detailed analysis of the performance at the level of each internal module. Implementation of new algorithms is improved using modeling, which offers the possibility of settings and corrections, before testing the prototypes and launching the production process. For more specific problems, the use of the models offers the possibility of novel solutions, if the usual configurations are not satisfactory.

## 2. CURRENT PROTECTION

The principle, consisting in the protection of the overcome of the limit values of the current, was the basis of the early protection systems. Starting from this basic principle, step maximum current protection systems have been developed. For an accurate operation of these relays, one must know the fault currents in each element of the grid [2, 3, 4].

The compulsory data for the relay settings are:

- ✓ the wiring diagram of the protected system, consisting in the protection relays and the associated current transformers;
- ✓ the impedances of the elements of the system (generators, transformers, transmission lines);
- ✓ minimum and maximum values of the short circuit currents in each protection location;
- ✓ starting currents of electric motors;
- ✓ maximum load current in each protection location;

- ✓ the decay curves of the fault current supplied by the generators;
- ✓ current transformers characteristics.

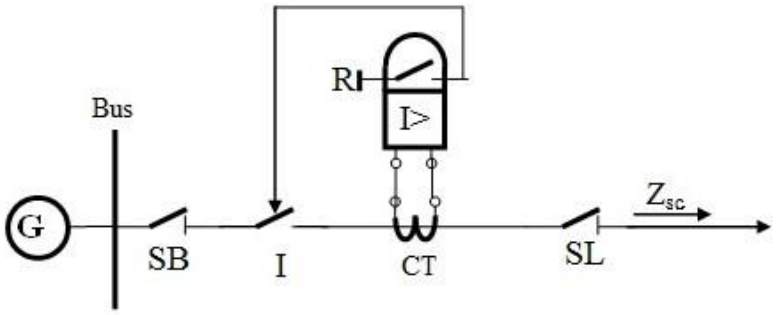


*Fig. 1. Maximum current protection schematics.*

The current relay settings must be checked in the first instance for the maximum value of the short circuit current. The reaction time must be minimum. Afterwards, the operation of the relay for minimum short circuit current must be checked. The reaction time must be satisfactory.

The wiring diagram of a maximum current protection for a radial network power system is depicted in *fig. 2*, where the bus insulator is denoted by SB, the line insulator, by SL, the breaker by I, the current transformer by TC and finally by *I*> the maximum current relay.

The main devices composing this protection system are the maximum current relays and the current transformers.

The tripping condition of the relay is:

$$I_c \geq I_p \tag{1}$$

where $I_c$ represents the current in the surveyed circuit and $I_p$ the tripping value of the relay, with respect to the primary winding of the current transformer. Note that this protection acts in a short circuit situation (instantaneous tripping with breaking) and doesn't fit for protection against overloads. The overload protection is also a current protection, but a delayed one. The delay is needed for discriminating between transient and permanent overloads, the overloads effects on the elements of the system being delayed in time.

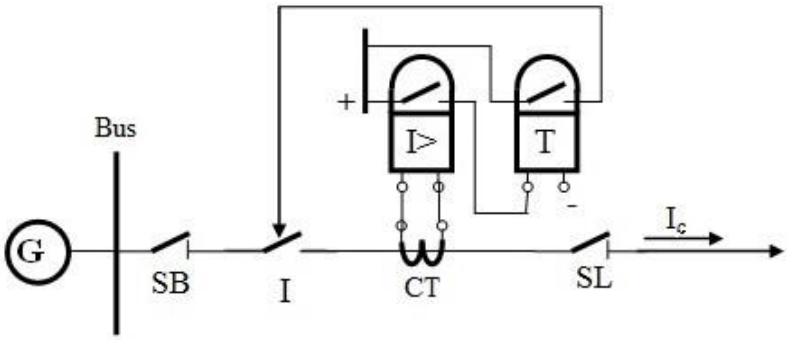


*Fig. 2. Overload protection relay schematics.*

Note that the contacts of the both relays, the maximum current relay *I*> and the time relay, perform a logic AND function. Consequently, the tripping of the breaker appears only if the current in the circuit overcomes the set value $I_p$ and the duration $t_c$ exceeds the delay time $t_p$:

$$\left(I_c > I_p\right)\text{and}\left(t_c > t_p\right) \tag{2}$$

Maximum current relays may present an independent characteristic curve, when the tripping time does not depend on the magnitude of the fault current, or a dependent one, when the tripping time depends on the magnitude of the surveyed circuit (which is a multiple of the set current). Consequently, this type of protection is characterized by the following features:

- ✓ the maximum current protection is the simplest and the cheapest protection (minimum number of components);
- ✓ the settings are pretentious and difficult to achieve in applications;
- ✓ readjustments and even relocating are needed in case of system modifications.

Protection must be selective in order to isolate the faulty area, leaving unaffected the rest of the system. In this respect, the protection device located nearest the faulty location must trip (i.e. the nearest fuse or breaker).

The correct coordination and the selectivity of the current protection may be achieved using several methods. The main possibilities in achieving selectivity are based on the following discrimination methods:

- ✓ discrimination by time;
- ✓ discrimination by current;
- ✓ discrimination fault direction;
- ✓ discrimination by both time and direction;
- ✓ discrimination by both time and current.

## 3. SECONDARY CURRENTS INJECTION DEVICE T 3000

A short circuit in the energy system imposes the isolation of the fault location with respect to the source, using commutation equipment. The electric arc occurring between the contacts, following the deionizing processes, determines a quick wearing of these equipment. If the short circuit duration is reduced, the protection system doesn't determine the disconnection, through the maximal delayed current relays.

The operation norms of the maximal delayed current relays impose that at several time intervals, the protection characteristics should be tested and set at the imposed values.

Checking the protective relays is made in laboratory, using secondary injection equipment (the authors of this paper have used the T/3000 [7, 8, 9] equipment, a complex verifying kit , *fig. 3*, permitting tests on all types of relays which can be tested on monophasic

faults, respectively all other possible tests on voltage and current transformers, on energy meters and on transducers as well.

The basic function of the equipment T/3000 is to generate currents and voltages, depending on the type of test, which is set on the LCD display.

The test results are stored in the internal memory of the equipment. These results can be subsequently transferred to a PC.

The equipment is provided with three generators:

- ✓ the main generator, having six outputs: high value alternating current, low value alternating current, low value direct current, current impulses, high alternating voltage source and low alternating voltage source;
- ✓ an auxiliary alternating voltage generator, generating an independent voltage phase adjustable;
- ✓ an auxiliary direct current generator used to feed relays under test.

All outputs are adjustable and metered on the large graphic LCD display. With the multi-purpose control knob and the graphic LCD display it is possible to enter the MENU mode that allows to control all functions and makes T3000 the most powerful testing device, with manual and automatic capabilities and with the possibility to transfer test results to a PC via the RS232 interface.

Other key features of the equipment are:

- ✓ oscilloscope function, permitting to display the measured current and voltage waveforms;
- ✓ other two independent measurement inputs for current and voltage, both with High and Low inputs, permitting the measurement of the output of current and voltage transformers and of any other sources;
- ✓ a print option of the saturation curve of the current transformer and other test results;
- ✓ an auxiliary output contact that follows Start and Stop inputs, allows simulating the circuit breaker.


*Fig. 3. Secondary currents injection kit T 3000.*

All the outputs of the T3000 kit are measured continuously. The waveform display function is useful in the case of distorted current or voltage.

In order to test the relays, it is important to use the set function of the injected power, due to the fact that the power of the nowadays relays is reduced. Because the current output is a voltage generator with low impedance, the adjustment of the low currents or of the injected currents on reduced loads is difficult because the operation in the initial area of the adjustment device is needed. The solution consists in reducing the available power in order to achieve a desired precision. Consequently the maximum voltage is reduced with a suitable factor.

The operator has different possibilities that permit to perform tests according to the characteristics of the relays. Some parameters, unused for a certain test are however visualized and saved. For instance, the auxiliary alternating voltage is also saved when a maximum current relay is saved, even though this function is not used.

For testing the transformers, there is a window for each type of test and the testing parameters are visualized and saved.

Each setting can be saved in the memory having the possibility to be reused afterwards. A fix number of tests can be saved and reused, the initial setting being that corresponding to the fault. The settings are continuously saved in the memory of the equipment, new settings being stored at the same address after the confirming requirement. In normal use, only the access to the standard settings is possible.

During the test, in the internal memory of the equipment can be saved up to 500 different tests. When a test is finalized, the settings along with the corresponding results can be stored in a personal computer where the X.PRO-3000 software is installed, which permits the revisualization of the results. When a PC is connected to the T3000 kit during the tests, the settings are available on the X.PRO-3000 interface.

Together with X.PRO-3000, the TDMS software is a powerful software package providing data management for acceptance and maintenance testing activities. Electrical apparatus data and test results are saved in the TDMS database for historical results analysis. TDMS software organize test data and results for the majority of electrical apparatus tested with ISA test sets and related software. TDMS software controls and provide data acquisition from all ISA Test.

TDMS has a built-in report editor that allows to generate professional test report for a single test object, for a group of tested devices or for an entire substation. It can create customized report or use standard forms. TDMS tests report can be exported in MS Office (Word and Excel), PDF or RTF formats.

TDMS is the control platform to run all ISA test software. Test programs, calibration, firmware, software upgrade and languages are all managed from TDMS.

The TDMS software platform allows the user to select easily and quickly the most appropriate software package for the required application. TDMS test software uses an open architecture easily expandable with additional software modules at any time.

TDMS package can be used to test any protective relays in: power generation plants, distribution and transmission networks and industry.

Manual control module has the following main characteristics:

- ✓ Intuitive graphic interface;
- ✓ Virtual front panel control;
- ✓ Graphical vector control;
- ✓ Ramp test: sequence of tests with ability to ramp any parameter up or down at the same time;
- ✓ Threshold test: automatic determination of threshold (current, voltage, frequency, phase angle);
- ✓ Rate of change (gradient) tests of frequency, voltage, current, phase angle and Vdc (Dx/Dt);
- ✓ Sequence editor;
- ✓ Test of distance relays with direct import of relay characteristics with RIO Format.
- ✓ Test of distance relays with simulation of all types of faults: single phase, two phase, two phase to ground, three phase;
- ✓ Report manager allows test report customization to user requirements;

Comrade Module permits:

- ✓ Playing back transient signals and waveform generation;
- ✓ Playing back transient signals from digital fault recorders and numerical relays;
- ✓ Analysis of relay operating time;
- ✓ Graphical view and replay of analog and binary signals;
- ✓ Impedance locus display;
- ✓ Scaling, cut, copy and paste of the analog signals.

The program Control Tab has a new layout, namely the relays Test Plan and Editor, which gives the user the possibility to create and run different test plan for different applications. The Plan Editor is available to create a test plan using predefined macro functions available for any type of relays. This new feature is particularly useful for testing multifunction relays.

The Test Plan can be associated to any relay in TDMS network structure and prior execution define relay setting and characteristic.

The Test Plan can be run on a specified relay: the entire test plan can be executed and/or the user can select the macros to execute on that relay according to its needs.

Finally, the Test Plan can be printed and saved automatically into the TDMS database.

## 4. EXPERIMENTAL RESULTS

Using the T3000 testing equipment the authors of the paper performed tests on several relays and current transformers.

The results of the tests, are displayed in the most simple cases using the internal memory using the section Results or using the software TDMS, *fig. 4-7*.

The Sequencer module is a software for determining the relays operating time and the logical sequence of the event.

- ✓ Overcurrent module for automatic testing of overcurrent relays, including all the standard curves IEEE and IEC [5, 6];
- ✓ Differential relays module, for automatic testing of differential relays (transformers, generators and bus bars);
- ✓ Line differential module, for automatic testing of line differential relays;
- ✓ Directional module, for testing of earth directional relays;
- ✓ Synchronizing module, for automatic testing of synchronizing devices with three or six voltages control;
- ✓ Swing Pro module, for testing power swing blocking and out of step function;
- ✓ Multifunction relays, which can be tested easily creating customized test plans;
- ✓ Harmonic generator module, allowing the creation of arbitrary harmonic waveform.

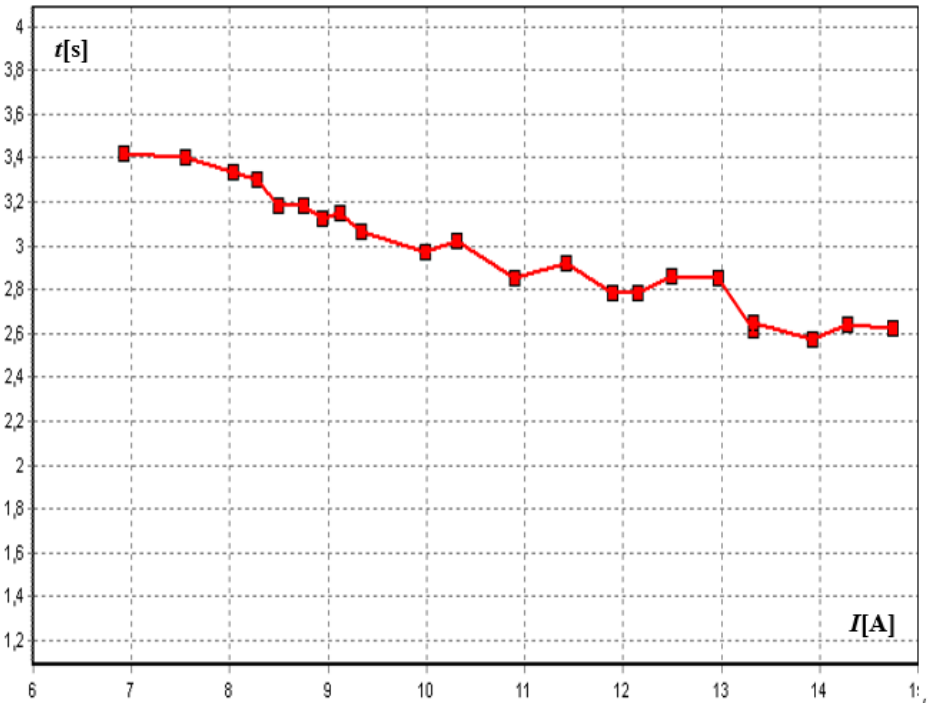


*Fig. 4. Maximal current time relay RTpC-1; Set to 2 s and 6 A.*

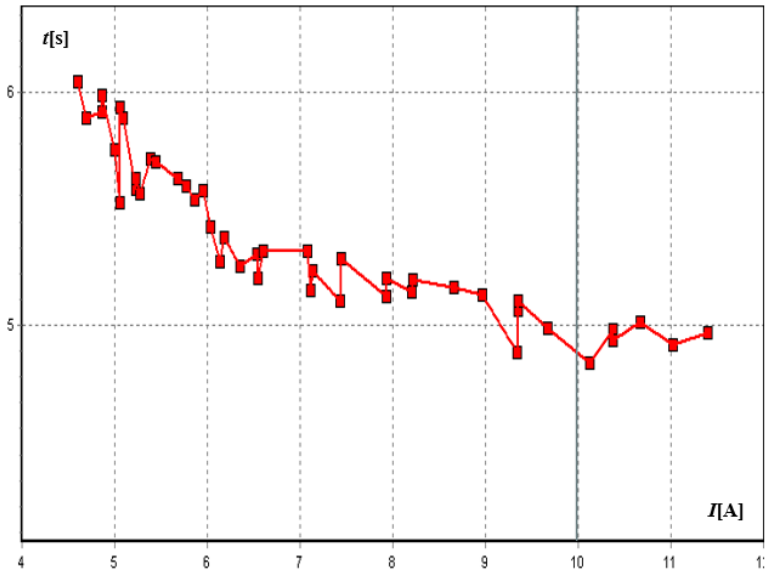


*Fig. 5. Maximal current time relay RTpC-1; Set to 4 s and 4 A.*

Taking into account the fact that the maximal time current relays permit a continuous setting of the timing, it is important that using the measuring kit to obtain an interdependent characteristic, as that presented in *fig. 8* for the RTpC-1 relay.

The maximal induction time relay are nowadays quite rarely used in protection systems, due to the interdependent time-current characteristics. A better performances version is represented by the protection scheme presented in *fig. 2*. The scheme is composed by a current relay along with a time relay, presenting an independent characteristics time-current.

The test equipment T 3000 permits the separate check of the two components of the protection system, the RC2 current relay and the RTPa-5 time relay, and in the same time determines the error of the measured value related to the setted value.

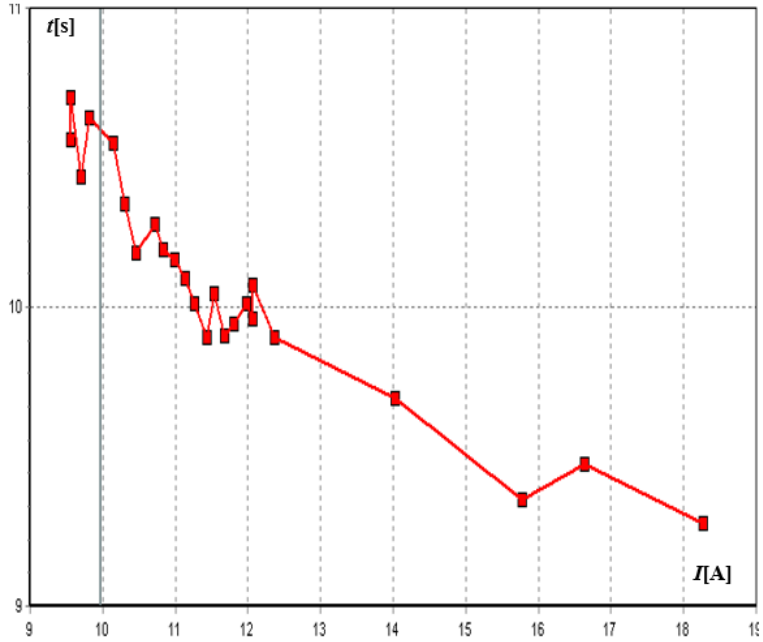


*Fig. 6. Maximal current time relay RTpC-1; Set to 8s and 8 A.*

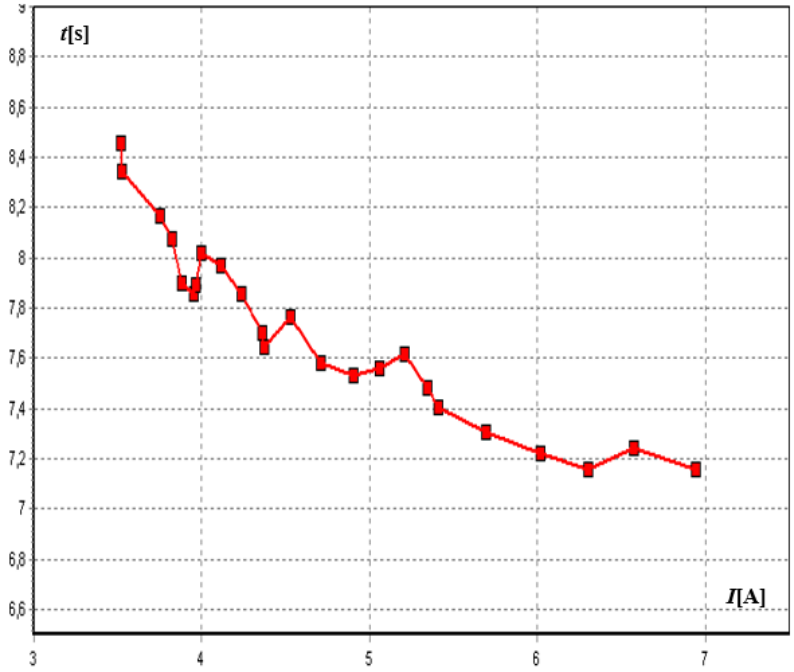


*Fig. 7. Maximal current time relay RTpC-1; Set to 6s and 3 A.*

## 5. CONCLUSIONS

Continuity in electric energy supply and the most rapid alleviation of the electric systems faults, in order to recover to a normal operating regime of these systems, means mostly a safe and a correct operation of the protective relays.

A key role in assuring these conditions have got the test equipment, used at the commissioning and the maintenance of the protection devices from the transformer stations and substations.

The choice of the appropriate measurement kit for verifying, testing, commissioning and maintenance is essential and must be considered in its technic and economic aspects.

In the choice of the T 3000 ISA TEST, the pros of this equipment have been considered, i.e. the checking possibility of all types of relays, of energy meters, of different transformers, along with the measurements of the earth resistivity, several ohmic tests, etc.

Using an equipment T 3000, equipped with a TDMS CT-VT-PT module in the measurements performed on a RTpC-1 induction relay, which have in their componence a transformer with eight outputs, is very suitable because this module permits recalling previous measurements saved in the internal memory of the equipment, displaying in real time the measured values and the relay characteristics, *fig. 8*, and in the same time processing the results of the measurements.

In the case of a maximal time – protection system having in its componence the a current relay RC2 and the time relay RTPa-5, the software package TDMS permits the automated computation of the errors and their storage in a graphic or a tabular form.

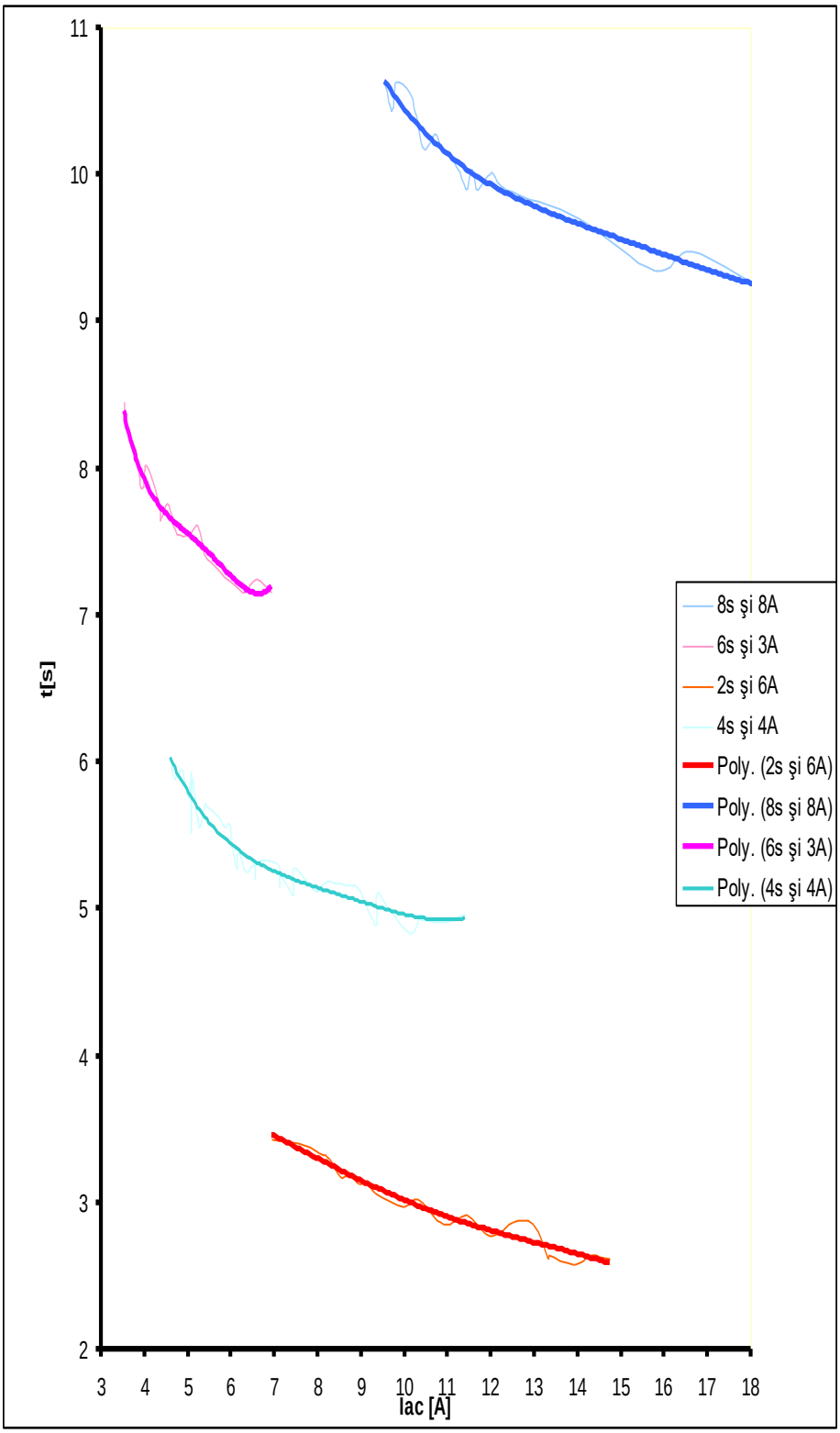


*Fig. 8. Maximal current time relay RTpC-1, i(t) dependent.*

It is however true that the tests for the mono phase faults are not sufficiently accurate. For these type of faults a more suitable test equipment should be used (for instance a secondary currents injection kit, like Mentor 3V3I [10]). This last kit can successfully replace the equipment presented previously.

*REFERENCES*

[1] Q. H. Wu, Z. Lu, T. Y. Ji, *Protective Relaying of Power Systems Using Mathematical Morphology*, Springer-Verlag London Limited, 2009.

[2] J. L. Blackburn, T. J. Domin, *Protective Relaying - Principles and Applications*, Taylor & Francis Group, LLC, 2007.

[3] W. A. Elmore, *Protective Relaying. Theory and Applications Second Edition*, Marcel Dekker Inc., 2004.

[4] J. Lewis Blackburn, *Protective Relaying*, Marcel Dekker Inc., 1987.

[5] IET, *Power System Protection: Volume 1 – Principles and Components - 2nd Edition*, Electricity Training Association, London 1995.

[6] IEEE, *Standard Dictionary of Electrical and Electronics Terms*, IEEE, Wiley Interscience, 1972.

[7] ISA, *Test Substation Maintenance and Commissioning Test Equipment*.

[8] *** www.isatest.com

[9] ISA, *Test T3000 Test Set, The Substation Equiment Test Set.*

[10] *** www.eurosmc.com

# DECLINE OF ACTIVE POWER LOSS BY IMPROVED MOTH-FLAME OPTIMIZATION ALGORITHM

Lenin **KANAGASABAI**
*Department of EEE, Prasad V. Potluri Siddhartha Institute of Technology,*
*Kanuru, Vijayawada, Andhra Pradesh -520007, India*
*gklenin@gmail.com*

**Keywords: Improved moth-flame optimization, Levy flight, optimal reactive power, transmission loss**

**Abstract:** *In this paper, Improved Moth-Flame Optimization (IMFO) algorithm has been proposed for solving Reactive power problem. Navigation method of moths in nature called transverse orientation is the key inspiration of the moth-flame algorithm (MFO). By maintaining a fixed angle with respect to the moon, Moths fly in the night and it's an effective mechanism for moths travelling in a straight line for long distances. Due to very slow convergence and poor precision, an improved version of MFO algorithm based on Levy-flight strategy has been proposed to solve the reactive power problem. The diversity of the population can be increased by Levy-flight to overcome premature convergence in order to reach the global optimal solution. This methodology improves the trade-off between exploration and exploitation ability of moth-flame algorithm (MFO).The proposed Improved Moth-Flame Optimization (IMFO) algorithm has been tested in standard IEEE 30,57,118 bus test systems and simulation results show clearly about the better performance of the proposed algorithm in reducing the real power loss with control variables within the limits.*

## 1. INTRODUCTION

To till date various methodologies has been applied to solve the Optimal Reactive Power problem. Many types of mathematical methodologies like linear programming, gradient method (Alsac et al., 1973; Lee et al., 1985; Monticelli et al., 1987; Deeb et al., 1990; Hobson, 1980; Lee et al., 1993; Mangoli et al., 1993; Canizares et al., 1996) [1-8] has been utilized to solve the reactive power problem, but those techniques found difficult in handling the constraints in the reactive power problem.. After that various types of evolutionary algorithms (Berizzi et al., 2012; Roy et al., 2012; Hu et al., 2010; Eleftherios et al., 2010) [9-12] has been applied to solve

the reactive power problem. But some algorithm good in exploration means, it lacks in exploitation and few algorithm's good in exploitation but lack in exploration. Speed of convergence is poor for some algorithms even though they got good trade-off between exploration and exploitation. In this paper, Improved Moth-Flame Optimization (IMFO) algorithm has been proposed for solving Reactive power problem. Navigation method of moths in nature called transverse orientation is the key inspiration of the moth-flame algorithm (MFO). By maintaining a fixed angle with respect to the moon, Moths fly in the night [13] and it's an effective mechanism for moths travelling in a straight line for long distances. Due to very slow convergence and poor precision, an improved version of MFO algorithm based on Levy-flight strategy has been proposed to solve the reactive power problem. The diversity of the population can be increased by Levy-flight to overcome premature convergence in order to reach the global optimal solution. This methodology improves the trade-off between exploration and exploitation ability of moth-flame algorithm (MFO).The proposed Improved Moth-Flame Optimization (IMFO) algorithm has been tested in standard IEEE 30, 57,118 bus test systems and simulation results show clearly about the better performance of the proposed algorithm in reducing the real power loss with control variables within the limits.

## 2. OBJECTIVE FUNCTION

### 2.1. Active power loss

Main objective of the reactive power dispatch problem is to minimize the active power loss and mathematically written by,

$$F = P_L = \sum_{k \in Nbr} g_k \left(V_i^2 + V_j^2 - 2V_i V_j \cos\theta_{ij}\right) \quad (1)$$

where*:* F - objective function, $P_L$ – power loss, $g_k$ – conductance of branch, $V_i$ and $V_j$ are voltages at buses i, j, Nbr - total number of transmission lines in power systems.

### 2.2. Voltage profile improvement

Objective function *F* has be rewritten to minimize the voltage deviation in PQ buses as follows,

$$F = P_L + \omega_v \times VD \quad (2)$$

where VD – voltage deviation, $\omega_v$- is a weighting factor of voltage deviation.

The Voltage deviation is given by:

$$VD = \sum_{i=1}^{Npq} |V_i - 1| \quad (3)$$

where Npq - number of load buses.

### 2.3. Equality Constraint

The power balance equation with respect to the equality constraint of the problem is written as follows:

$$P_G = P_D + P_L \quad (4)$$

where $P_G$- total power generation, $P_D$ - total power demand.

### 2.4. Inequality Constraints

The inequality constraint with upper and lower bounds on the active power of slack bus ($P_g$), and reactive power of generators ($Q_g$) are written as follows:

$$P_{gslack}^{min} \leq P_{gslack} \leq P_{gslack}^{max} \quad (5)$$

$$Q_{gi}^{min} \leq Q_{gi} \leq Q_{gi}^{max}, i \in N_g \quad (6)$$

Upper and lower bounds on the bus voltage magnitudes ($V_i$) is given by:

$$V_i^{min} \leq V_i \leq V_i^{max}, i \in N \quad (7)$$

Upper and lower bounds on the transformers tap ratios ($T_i$) is given by:

$$T_i^{min} \leq T_i \leq T_i^{max}, i \in N_T \quad (8)$$

Upper and lower bounds on the compensators ($Q_c$) is given by:

$$Q_c^{min} \leq Q_c \leq Q_C^{max}, i \in N_C \quad (9)$$

where N is the total number of buses, $N_g$ is the total number of generators, $N_T$ is the total number of Transformers, $N_c$ is the total number of shunt reactive compensators.

## 3. MOTH-FLAME OPTIMIZATION (MFO) ALGORITHM

Moth-flame optimization algorithm is based on the simulation of the behaviour of moths which has special navigation methods in night. Navigation method of moths in nature called transverse orientation is the key inspiration of the moth-flame algorithm (MFO).

By maintaining a fixed angle with respect to the moon, Moths fly in the night and it's an effective mechanism for moths travelling in a straight line for long distances. Set of moths is represented in a matrix N in the MFO algorithm. There is an array $O$N for all the moths, to store the corresponding fitness values. Flames are other one of key components in the moth-flame algorithm.

It is also assumed that there is an array $O$L for the flames, a matrix S similar to the moth matrix is considered to store the corresponding fitness values.

Three-tuple in MFO algorithm defined as follows:

$$MFO = (Q, G, H) \tag{10}$$

An arbitrary population of moths is created by the function Q. Q function mathematical model is given is as follows:

$$Q: \emptyset \rightarrow \{N, ON\} \tag{11}$$

Moths move around the exploration space on basis of G function. G function received the matrix of N and returns its modernized one ultimately:

$$G: N \rightarrow N \tag{12}$$

When the termination criterion is satisfied H function returns true and it will be false when termination criterion is not satisfied:

$$H: N \rightarrow \{True, False\} \tag{13}$$

MFO algorithm is defined as follows, with Q, G, and H, as the general framework:

*N = ( );*

*When (N) is equal to false condition, then: N = (N)*

*End.*

$P$ Function is iteratively run after the initialization, until the H function returns true.

When simulating the behaviour of moths mathematically, with respect to a flame the

position of each moth is updated using the following equation:

$$N_i = SL(N_i, Fl_j) \tag{14}$$

The $i$th moth indicated by $N_i$, $j$th flame indicated by $Fl_j$, and $S$L imply the spiral function.

Spirals are utilized by following conditions: (a) initial point of the Spiral's should start from the moth; (b) final point of the Spiral's should be the position of the flame; (c) in the search space fluctuation range of spiral should not exceed the space limit.

Considering these points, a logarithmic spiral is defined for the MFO algorithm as follows:

$$SL(N_i, Fl_j) = DT_i \cdot e^{bt} \cdot cos(2\pi ft) + Flj \tag{15}$$

Distance of the $i$th moth for the $j$th flame is indicated by $DT_i$, for defining the shape of the logarithmic spiral $b$ is a constant, and $t$ is an arbitrary number in the range [−1, 1].

Calculation of $D$T is as follows:

$$DT_i = \left|Fl_j - N_i\right| \tag{16}$$

where $N_i$ indicate the $i$th moth, $Fl_j$ indicates the $j$th flame, and $DT_i$ indicates the distance of the $i$th moth for the $j$th flame. Spiral flying path of moths described by Equation (16). The next position of a moth is defined with respect to a flame by equation (16).

In the spiral equation the $t$ parameter defines how much the next position of the moth should be close to the flame ($t = -1$ is the closest position to the flame, while $t$=1 shows the farthest). Position updating in equation (15) requires the moths to move towards a flame, & it lead to be trapped in local optima quickly.

Each moth is obliged to update its position using only one of the flames by equation (15) to prevent trap in local optima. In the search space the position updating of moths with respect to $n$ different locations may degrade the exploitation to reach best promising solutions. An adaptive mechanism is provided to the number of flame to resolve degrade problem & it done by following equation,

$$Flame\ number = round\ \left(K - l * \frac{K-cn}{IN}\right) \tag{17}$$

The current number of iteration is given by cn, maximum number of flames indicated by K, and the maximum number of iterations by IN. Exploration and exploitation of the search space is perfectly balanced by gradual decrement in number of flames.

*Position of moths has been initialized*
*While (Iteration <= Max iteration);*
*By equation (17) update the flame number*
*ON = Fitness Function (N);*
*If iteration = = 1*
*FI = sort (N); OFI = sort(ON);*
*Else*
*FI = sort ($N_t - 1$, $N_t$); OFI = sort($N_{t-1}$, $N_t$);*
*End*
*For i=1:n ; For j=1:d*
*Modernize r and t*
*By equation (16) calculate DT using with respect to the corresponding moth*
*By equations (14) and (15) renew (i, j) with respect to the corresponding moth*
*End End.*

## 4. LEVY-FLIGHT

Animals look for food in arbitrary manner, as moving place to place. The choice of the direction relies only on a mathematical model [15], which is called Levy- flight & it have been applied to optimization problems which show its promising capability [14,15].Mathematically exclamation, an easy version of Levy distribution can be defined as [14],

$$L(s,\gamma,\mu) = \begin{cases} \sqrt{\frac{\gamma}{2\pi}} & exp\left[-\frac{\gamma}{2(s-\mu)}\right]\frac{1}{(s-\mu)^{3/2}} \quad if\ 0 < \mu < s < \infty \\ 0 \quad if\ s \le 0 \end{cases} \tag{18}$$

where $\gamma > 0$ parameter is scale (controls the scale of distribution) parameter, $\mu$ parameter is location or shift parameter. In general, Levy distribution should be defined in terms of Fourier transform as follows [14],

$$F(k) = exp\left[-\alpha|k|^{\beta}\right], 0 < \beta \le 2 \tag{19}$$

where $\alpha$ is a parameter within [-1,1] interval and known as scale factor. By Levy flight, new-fangled state of the particle is designed as [15],

$$X^{t+1} = X^t + \alpha \oplus Levy\ (\beta) \tag{20}$$

$\alpha$ is the step size which must be related to the scales of the problem of interest.

In the proposed method $\alpha$ is arbitrary number for all dimensions of particles [14].

$$X^{t+1} = X^t + random\left(size(D)\right) \oplus Levy(\beta) \tag{21}$$

The product $\oplus$ means entry-wise multiplications. A non-trivial scheme of generating step size s samples are summarized as follows [14],

$$X^{t+1} = X^t + random\left(size(D)\right) \oplus Levy(\beta) \sim 0.01 \frac{u}{|v|^{1/\beta}}\left(x_j^t - gb\right) \tag{22}$$

where *u* and *v* are drawn from the normal distributions. That is [15],

$$u \sim N(0, \sigma_u^2) \quad v \sim N(0, \sigma_v^2) \tag{23}$$

with

$$\sigma_u = \left\{\frac{\Gamma(1+\beta)sin(\pi\beta/2)}{\Gamma[(1+\beta)/2]\beta 2^{(\beta-1)/2}}\right\}^{1/\beta}, \sigma_v = 1 \tag{24}$$

Here $\Gamma$ is standard Gamma function. While performing distribution by Levy flights [14] is the value taken by the $\beta$ parameter and it substantially affects distribution.

## 5. PROPOSED IMPROVED MOTH- FLAME (IMFO) OPTIMIZATION ALGORITHM

Proposed IMFO algorithm‘s global search ability is strengthened using arbitrary walk with help of Levy-flight to eliminate the weakness of MFO algorithm [13] Improved Moth-flame algorithm (IMFO) for solving Reactive power problem given below.

*Position of moths has been initialized*
*While (Iteration <= Max iteration) ; By equation (17) update the flame number*
*ON = Fitness Function (N);*
*If iteration = = 1*
*Fl = sort (N); OFl = sort(ON);*
*Else*
*Fl = sort ($N_t - 1$, $N_t$); OFl = sort($N_{t-1}$, $N_t$);*
*End*
*For i=1:n ; For j=1:d*

*Modernize $r$ and $t$*

*By equation (16) calculate $\Delta T$ using with respect to the corresponding moth*

*By equations (14) and (15) renew $(i, j)$ with respect to the corresponding moth*

*End*

*For each search agent renew the position of the existing search agent by using Levy-flight*

*End*

*When Iteration = Iteration + 1;*

*End*

## 6. SIMULATION RESULTS

In standard IEEE 30-bus, 41 branch system validity of proposed Improved Moth-Flame Optimization (IMFO) algorithm has been verified and the system has 6 generator-bus voltage magnitudes, 4 transformer-tap settings, and 2 bus shunt reactive compensators. 2, 5, 8, 11 and 13 are considered as PV generator buses, Bus 1 is taken as slack bus and others are PQ load buses. Primary variables limits are given in *Table 1*.

*Table 1. Primary Variable Limits (Pu)*

| *List of Variables* | *Minimum* | *Maximum* | *group* |
|---|---|---|---|
| *Generator Bus* | *0.95* | *1.1* | *Continuous* |
| *Load Bus* | *0.95* | *1.05* | *Continuous* |
| *Transformer-Tap* | *0.9* | *1.1* | *Discrete* |
| *Shunt Reactive Compensator* | *-0.11* | *0.31* | *Discrete* |

In *Table 2* the power limits of generators buses are listed.

*Table 2. Generators Power Limits*

| *Bus* | *Pg* | *Pgminimum* | *Pgmaximum* | *Qgminimum* | *Qmaximum* |
|---|---|---|---|---|---|
| *1* | *96.00* | *49* | *200* | *0* | *10* |
| *2* | *79.00* | *18* | *79* | *-40* | *50* |
| *5* | *49.00* | *14* | *49* | *-40* | *40* |
| *8* | *21.00* | *11* | *31* | *-10* | *40* |
| *11* | *21.00* | *11* | *28* | *-6* | *24* |
| *13* | *21.00* | *11* | *39* | *-6* | *24* |

*Table 3* shows the proposed Improved Moth-Flame Optimization (IMFO) algorithm successfully kept the control variables within limits.

*Table 4* narrates about the performance of the proposed Improved Moth-Flame Optimization (IMFO) algorithm.

*Fig 1* shows about the voltage deviations during the iterations and Table 5 list out the overall comparison of the results of optimal solution obtained by various methods.

*Table 3. After optimization values of control variables*

| *List of Control Variables* | *IMFO* |
|---|---|
| *V1* | *1.0512* |
| *V2* | *1.0434* |
| *V5* | *1.0297* |
| *V8* | *1.0382* |
| *V11* | *1.0735* |
| *V13* | *1.0529* |
| *T4,12* | *0.00* |
| *T6,9* | *0.01* |
| *T6,10* | *0.90* |
| *T28,27* | *0.91* |
| *Q10* | *0.10* |
| *Q24* | *0.10* |
| *Real power loss* | *4.2898* |
| *Voltage deviation* | *0.9090* |

*Table 4. Performance of IMFO algorithm*

| *Iterations* | *25* |
|---|---|
| *Time taken (secs)* | *7.89* |
| *Real power loss* | *4.2898* |

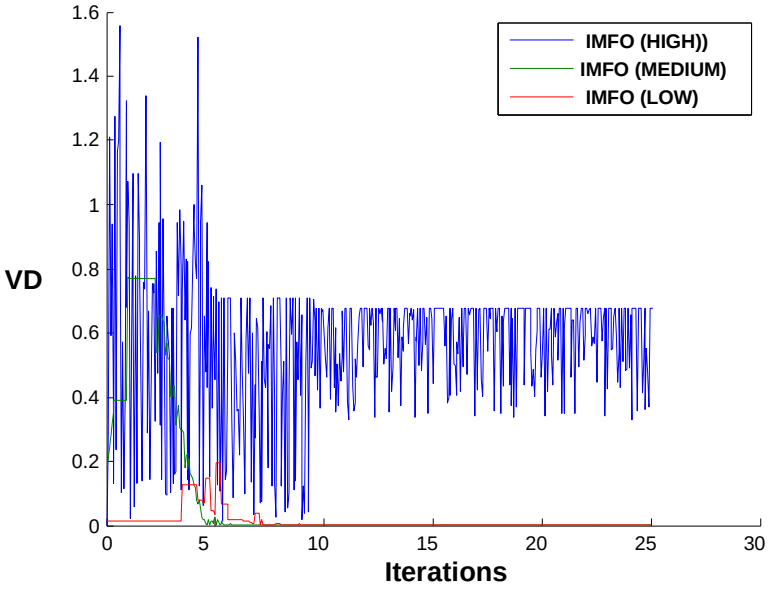


*Fig. 1. Voltage deviation (VD) characteristics*

*Table 5. Comparison of results*

| *List of Techniques* | *Real power loss (MW)* |
|---|---|
| *SGA(Wu et al., 1998) [16]* | *4.98* |
| *PSO(Zhao et al., 2005) [17]* | *4.9262* |
| *LP(Mahadevan et al., 2010) [18]* | *5.988* |
| *EP(Mahadevan et al., 2010) [18]* | *4.963* |
| *CGA(Mahadevan et al., 2010) [18]* | *4.980* |
| *AGA(Mahadevan et al., 2010) [18]* | *4.926* |
| *CLPSO(Mahadevan et al., 2010) [18]* | *4.7208* |
| *HSA (Khazali et al., 2011) [19]* | *4.7624* |
| *BB-BC (Sakthivel et al., 2013) [20]* | *4.690* |
| *MCS(Tejaswini sharma et al.,2016) [21]* | *4.87231* |
| *Proposed IMFO* | *4.2898* |

At that Improved Moth-Flame Optimization (IMFO) algorithm has been tested in standard IEEE-57 bus power system. The reactive power compensation buses are 18, 25 and 53. Bus 2, 3, 6, 8, 9 and 12 are PV buses and bus 1 is selected as slack-bus. The system variable limits are given in *Table 6*.

The preliminary conditions for the IEEE-57 bus power system are given as follows:
Pload = 12.129 p.u. Qload = 3.069 p.u.

The total initial generations and power losses are obtained as follows:
$\sum P_G$ = 12.471 p.u. $\sum Q_G$ = 3.3160 p.u.
Ploss = 0.25875 p.u. Qloss = -1.2074 p.u.

*Table 6. Variable Limits*

| *Reactive Power Generation Limits* | | | | | | | |
|---|---|---|---|---|---|---|---|
| *Bus no* | *1* | *2* | *3* | *6* | *8* | *9* | *12* |
| *Qgmin* | *-1.4* | *-.015* | *-.02* | *-0.04* | *-1.3* | *-0.03* | *-0.4* |
| *Qgmax* | *1* | *0.3* | *0.4* | *0.21* | *1* | *0.04* | *1.50* |

| *Voltage And Tap Setting Limits* | | | | | |
|---|---|---|---|---|---|
| *vgmin* | *Vgmax* | *vpqmin* | *Vpqmax* | *tkmin* | *tkmax* |
| *0.9* | *1.0* | *0.91* | *1.05* | *0.9* | *1.0* |

| *Shunt Capacitor Limits* | | | |
|---|---|---|---|
| *Bus no* | *18* | *25* | *53* |
| *Qcmin* | *0* | *0* | *0* |
| *Qcmax* | *10* | *5.2* | *6.1* |

*Table 7* shows the various system control variables i.e. generator bus voltages, shunt capacitances and transformer tap settings obtained after optimization which are within the acceptable limits. In Table 8, shows the comparison of optimum results obtained from proposed methods with other optimization techniques. These results indicate the robustness of proposed approaches for providing better optimal solution in case of IEEE-57 bus system.

*Table 7. Control variables obtained after optimization*

| *Control Variables* | *IMFO* |
|---|---|
| *V1* | *1.10* |
| *V2* | *1.039* |
| *V3* | *1.038* |
| *V6* | *1.027* |
| *V8* | *1.029* |
| *V9* | *1.006* |
| *V12* | *1.011* |
| *Qc18* | *0.0664* |
| *Qc25* | *0.200* |
| *Qc53* | *0.0476* |
| *T4-18* | *1.004* |
| *T21-20* | *1.043* |
| *T24-25* | *0.861* |
| *T24-26* | *0.876* |
| *T7-29* | *1.057* |
| *T34-32* | *0.879* |
| *T11-41* | *1.011* |
| *T15-45* | *1.030* |
| *T14-46* | *0.910* |
| *T10-51* | *1.020* |
| *T13-49* | *1.060* |
| *T11-43* | *0.910* |
| *T40-56* | *0.900* |
| *T39-57* | *0.950* |
| *T9-55* | *0.950* |

*Table 8. Comparison results*

| *S.No.* | *Optimization Algorithm* | *Finest Solution* | *Poorest Solution* | *Normal solution* |
|---|---|---|---|---|
| *1* | *NLP [22]* | *0.25902* | *0.30854* | *0.27858* |
| *2* | *CGA [22]* | *0.25244* | *0.27507* | *0.26293* |

| | | | | |
|---|---|---|---|---|
| *3* | *AGA [22]* | *0.24564* | *0.26671* | *0.25127* |
| *4* | *PSO-w [22]* | *0.24270* | *0.26152* | *0.24725* |
| *5* | *PSO-cf [22]* | *0.24280* | *0.26032* | *0.24698* |
| *6* | *CLPSO [22]* | *0.24515* | *0.24780* | *0.24673* |
| *7* | *SPSO-07 [22]* | *0.24430* | *0.25457* | *0.24752* |
| *8* | *L-DE [22]* | *0.27812* | *0.41909* | *0.33177* |
| *9* | *L-SACP-DE [22]* | *0.27915* | *0.36978* | *0.31032* |
| *10* | *L-SaDE [22]* | *0.24267* | *0.24391* | *0.24311* |
| *11* | *SOA [22]* | *0.24265* | *0.24280* | *0.24270* |
| *12* | *LM [23]* | *0.2484* | *0.2922* | *0.2641* |
| *13* | *MBEP1 [23]* | *0.2474* | *0.2848* | *0.2643* |
| *14* | *MBEP2 [23]* | *0.2482* | *0.283* | *0.2592* |
| *15* | *BES100 [23]* | *0.2438* | *0.263* | *0.2541* |
| *16* | *BES200 [23]* | *0.3417* | *0.2486* | *0.2443* |
| *17* | *Proposed IMFO* | *0.22092* | *0.23016* | *0.22268* |

Then Improved Moth-Flame Optimization (IMFO) algorithm has been tested in standard IEEE 118-bus test system [24].The system has 54 generator buses, 64 load buses, 186 branches and 9 of them are with the tap setting transformers. The limits of voltage on generator buses are 0.95 -1.1 per-unit., and on load buses are 0.95 -1.05 per-unit. The limit of transformer rate is 0.9 -1.1, with the changes step of 0.025. The limitations of reactive power source are listed in *Table 9*, with the change in step of 0.01.

*Table 9. Limitation of reactive power sources*

| *BUS* | *5* | *34* | *37* | *44* | *45* | *46* | *48* |
|---|---|---|---|---|---|---|---|
| *QCMAX* | *0* | *14* | *0* | *10* | *10* | *10* | *15* |
| *QCMIN* | *-40* | *0* | *-25* | *0* | *0* | *0* | *0* |
| *BUS* | *74* | *79* | *82* | *83* | *105* | *107* | *110* |
| *QCMAX* | *12* | *20* | *20* | *10* | *20* | *6* | *6* |
| *QCMIN* | *0* | *0* | *0* | *0* | *0* | *0* | *0* |

The statistical comparison results of 50 trial runs have been list in *Table 10* and the results clearly show the better performance of proposed Improved Moth-Flame Optimization (IMFO) algorithm in reducing the real power loss.

*Table 10. Comparison results*

| *Active power loss (MW)* | *BBO [25]* | *ILSBBO/ strategy1 [25]* | *ILSBBO/ strategy 2 [25]* | *Proposed IMFO* |
|---|---|---|---|---|

| | | | | |
|---|---|---|---|---|
| *Min* | *128.77* | *126.98* | *124.78* | *117.64* |
| *Max* | *132.64* | *137.34* | *132.39* | *121.72* |
| *Average* | *130.21* | *130.37* | *129.22* | *118.32* |

## 7. CONCLUSION

In this paper, Improved moth-flame optimization (IMFO) algorithm been successfully implemented to solve Optimal Reactive Power Dispatch problem. An improved version of MFO algorithm based on Levy-flight strategy has been solved the reactive power problem. The diversity of the population can be increased by Levy-flight to overcome premature convergence in order to reach the global optimal solution. This methodology improved the trade-off between exploration and exploitation ability of moth-flame algorithm (MFO).The proposed IMFO algorithm has been tested in the standard IEEE 30, 57,118 bus systems. Simulation results show that IMFO provided better optimal solution in decreasing the real power loss. The control variables obtained after the optimization by IMFO are well within the limits.

## *REFERENCES*

[1] O. Alsac and B. Scott, *Optimal load flow with steady state security*, IEEE Transaction. PAS, pp. 745-751, 1973.

[2] K.Y. Lee, Y.M Paru, J.L Oritz, *A united approach to optimal real and reactive power dispatch*, IEEE Transactions on power Apparatus and systems, PAS-104 : 1147-1153, 1985.

[3] A. Monticelli, M.V.F Pereira and S. Granville, *Security constrained optimal power flow with post contingency corrective rescheduling* , IEEE Transactions on Power Systems :PWRS-2, No. 1, pp.175-182, 1987.

[4] N. Deeb, S.M. Shahidehpur, *Linear reactive power optimization in a large power network using the decomposition approach*, IEEE Transactions on power system, 5(2), pp. 428-435, 1990.

[5] E. Hobson, *Network consrained reactive power control using linear programming*, IEEE Transactions on power systems PAS -99 (4), pp 868-877, 1980.

[6] K. Y Lee, Y. M Park and J. L Oritz, *Fuel –cost optimization for both real and reactive power dispatches*, IEE Proc; 131C,(3), pp.85-93, 1993.

[7] M. K Mangoli and K.Y. Lee, *Optimal real and reactive power control using linear programming*, Electr. Power, Syst. Res, vol.26, pp.1-10, 1993.

[8] C. A Canizares, A. C. Z. de Souza and V. H. Quintana, *Comparison of performance indices for detection of proximity to voltage collapse*, vol. 11, no.3, pp.1441-1450, 1996.

[9] A. Berizzi, C. Bovo, M. Merlo and M. Delfanti, *A GA approach to compare orpf objective functions including secondary voltage regulation*, Electric Power Systems Research, vol. 84, no. 1, pp. 187 – 194, 2012.

[10] P. Roy ,S. Ghoshal and S. Thakur, *Optimal var control for improvements in voltage profiles and for real power loss minimization using biogeography based optimization*, International Journal of Electrical Power and Energy Systems, vol. 43, no. 1, pp. 830 – 838, 2012.

[11] Z. Hu, X.Wang and G. Taylor, *Stochastic optimal reactive power dispatch: Formulation and solution method*, International Journal of Electrical Power and Energy Systems, vol. 32, no. 6, pp. 615 – 621, 2010.

[12] E. I. Amoiralis, P. S. Georgilakis, Marina A. Tsili, A. G. Kladas, *Ant Colony Optimisation solution to distribution transformer planning problem*, Internationl Journal of Advanced Intelligence Paradigms , vol.2, no.4 ,pp.316 – 335, 2010.

[13] S. Mirjalili, *Moth-flame optimization algorithm: a novel nature-inspired heuristic paradigm*, Knowledge-Based Systems, vol. 89, pp. 228–249, 2015.

[14] A. F. Kamaruzaman, A. M. Zain, S. M. Yusuf, and A. Udin, *Levy flight algorithm for optimization problems—a literature review*, Applied Mechanics and Materials, vol. 421, pp. 496–501, 2013.

[15] P. Barthelemy, J. Bertolotti, and D. S. Wiersma, *A Levy flight for light, Nature*, vol. 453, no. 7194, pp. 495–498, 2008.

[16] Q. H. Wu, Y. J. Cao, and J. Y.Wen, *Optimal reactive power dispatch using an adaptive genetic algorithm*, Int. J. Elect. Power Energy Syst, vol 20, pp. 563-569, 1998.

[17] B. Zhao, C. X. Guo and Y. J. CAO, *Multiagent-based particle swarm optimization approach for optimal reactive power dispatch*, IEEE Trans. Power Syst. vol. 20, no. 2, pp. 1070-1078, 2005.

[18] K. Mahadevan, P.S. Kannan, *Comprehensive Learning Particle Swarm Optimization for Reactive Power Dispatch*, Applied Soft Computing, vol. 10, no. 2, pp. 641–52, 2010.

[19] .A. H. Khazali, M. Kalantar, *Optimal Reactive Power Dispatch based on Harmony Search Algorithm*, Electrical Power and Energy Systems, vol. 33, no. 3, pp. 684–692, 2011.

[20] S. Sakthivel, M. Gayathri, V. Manimozhi, *A Nature Inspired Optimization Algorithm for Reactive Power Control in a Power System*, International Journal of Recent Technology and Engineering, pp. 29-33, vol.2, issue 1, 2013.

[21] T. Sharma, L. Srivastava, S. Dixit, *Modified Cuckoo Search Algorithm For Optimal Reactive Power Dispatch*, Proceedings of 38 th IRF International Conference, Chennai, India, pp. 4-8, 2016.

[22] C. Dai, W. Chen, Y. Zhu, and X. Zhang, *Seeker optimization algorithm for optimal reactive power dispatch*, IEEE Trans. Power Systems, vol. 24, no. 3, pp. 1218-1231, 2009.

[23] J. R. Gomes and 0. R. Saavedra, *Optimal reactive power dispatch using evolutionary computation: Extended algorithms*, IEE Proc. - Gener. Transm. Distrib, vol. 146, no. 6, 1999.

[24] IEEE, *The IEEE 30-bus test system and the IEEE 118-test system*, http://www.ee.washington.edu/trsearch/pstca/., 1993.

[25] J. Cao, F. Wang and P. Li, *An Improved Biogeography-based Optimization Algorithm for Optimal Reactive Power Flow*, International Journal of Control and Automation vol. 7, no. 3 , pp. 161-176, 2014.

# BIOT-SAVART LAW APPLICATION IN WIRELESS POWER TRANSFER – DEPENDENCE OF MAGNETIC FIELD TO ANGLE POSITION

Bogdan **IUGA,** Radu-Adrian **TIRNOVAN**
*Technical University of Cluj-Napoca, Romania*
*bogdan_i2008@yahoo.com*

**Keywords: Biot-Savart law, exterior magnetic field, closed loop**

**Abstract:** *The magnetic field of a closed loop of conductive wire can be computed due to Biot-Savart law, which analyses the value of the field at an exterior point from the transversal axis. If the measure point is out of the axis then the magnetic field has completely different values. A general stated form of this law can measure the value in any point, in relation to Euclidian distance from the loop.*

## 1. INTRODUCTION

In electromagnetics, main fact that limits this sector is the magnetic field, a basic component that "runs out" in free space. Since the discovery of the electricity, scientists made numerous researches in magnetic field domain and most of the results are in use today. One of the most important laws that refer to magnetic field induction computation is the Biot-Savart law.

Biot-Savart law was formulated by Jean-Baptiste Biot and Félix Savart around 1820 and is the fundamental law for computing magnetic field. It corresponds to Coulomb's law for calculating the electric field. The Biot-Savart law is an equation describing the magnetic field generated by an electric current as a vector that has magnitude, direction and length [1].

If all the properties of the magnetic field are known, then it is simple to calculate possible energy transfer between devices.

The aim of this work consists in analyzing the computation of magnetic field induction produced by a closed loop of a conducting wire. The general formula is referring to an ideal case when the magnetic induction is calculated in the axis of the loop. In real cases, there are

always angular deviations, which determine directly modifications of the magnetic field induction values.

## 2. MATHEMATICAL ANALYSIS

The magnetic induction is a vector, so its calculation involves to take in consideration the vector properties and Cartesian distribution of its components.

The general expression of the Biot-Savart law is referring to the magnetic field of a conductive wire and it states that variable currents give rise to magnetic field. Take in account a single conductor, passed by the current *I*, the magnetic induction at any point *P* can be calculated summing the contributions $d\vec{B}$ of all the infinitesimal $d\vec{S}$ elements [2]:

$$d\vec{B} = \frac{\mu_0}{4\pi} \cdot \frac{I \cdot d\vec{S} \times \hat{r}}{r^2} \tag{1}$$

where:

- $d\vec{S}$ is a vector with the magnitude equal to the length of the analyzed segment and with same direction as the current I. In this case, I become a finite elementary current source;
- $r$ is the Euclidian distance from the source to the measuring point;
- $\hat{r}$ is the versor of the corresponding vector [3].

When the conducting wire is coiled around an axis (wire loop) the magnetic induction computation becomes complicated. Major modifications are made on vector $d\vec{S}$. In figure is illustrated the connections between the vectors involved in magnetic induction calculation for a wire loop.

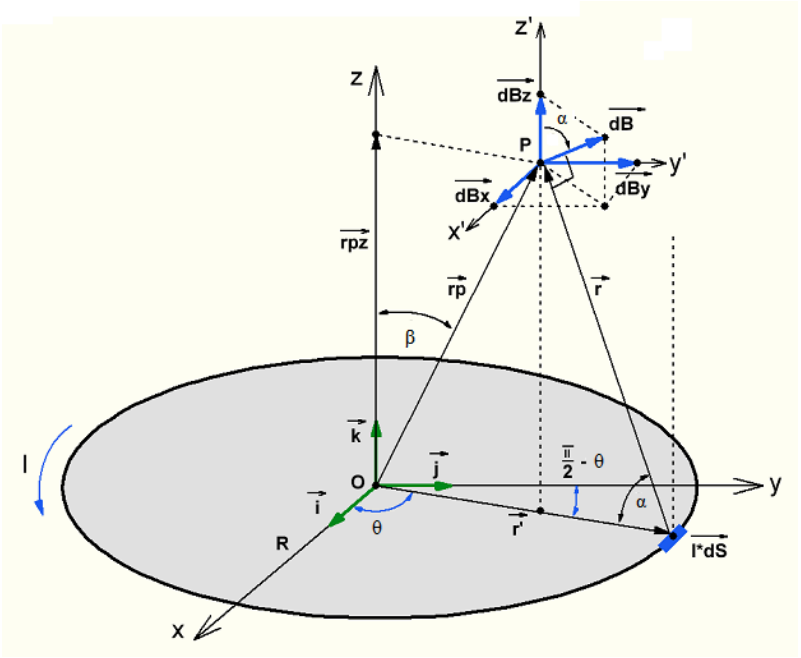


*Fig. 1 Explained for magnetic induction calculation for a single wire loop.*

$I \cdot d\vec{S}$ is considered the current carrying element and because the loop is a circle, the location is given by the $\vec{r}'$. In Cartesian coordinates (x, y, z), the vector $\vec{r}'$ is the sum of his axis components [3]:

$$\vec{r'} = \vec{r_x'} + \vec{r_y'} = R \cdot \cos\theta \cdot \hat{i} + R \cdot \sin\theta \cdot \hat{j} \tag{2}$$

where:

- $R$ is the radius of the circle wire loop;
- $\theta$ is the angle with x axis;
- $\hat{i}, \hat{j}, \hat{k}$ are the versors of the *x* axis, *y* axis, respectively of *z* axis of the Cartesian coordinates system.

To determine the value of current element, the source element has been derivate in relation with angle of rotation [4]:

$$\begin{aligned} I \cdot d\vec{S} &= I \cdot \left( \frac{d}{d\theta} \vec{r'} \right) \cdot d\theta = I \cdot d\theta \cdot R \cdot \frac{d}{d\theta} \left( \cos\theta \cdot \hat{i} + \sin\theta \cdot \hat{j} \right) = \\ &= I \cdot d\theta \cdot R \left( -\sin\theta \cdot \hat{i} + \cos\theta \cdot \hat{j} \right) \end{aligned} \tag{3}$$

To measure the value of the magnetic field in a specific point, the point must be located. In *xOyOz* coordinates the point has the coordinates notation *P(x, y, z)* and is characterized by the vector position [3]:

$$\vec{r_P} = x \cdot \hat{i} + y \cdot \hat{j} + z \cdot \hat{k} \tag{4}$$

but in the same time, this vector is the sum of his contribution on the axis:

$$\vec{r_P} = \vec{r_{Px}} + \vec{r_{Py}} + \vec{r_{Pz}} \tag{5}$$

So, the position vector can be described from his relation with the contributions from any axis, for example z axis [3]:

$$\vec{r_P} = \frac{\vec{r_{Pz}}}{\cos\beta} = \frac{z}{\cos\beta} \cdot \hat{k} \tag{6}$$

Heaving all components from the vector triangle, the Euclidian distance from the source to the measuring point can be calculated [4]:

$$d\vec{r} = \vec{r_P} - \vec{r'} \tag{7}$$

$$\vec{r} = \frac{z}{\cos\beta} \cdot \hat{k} - R \cdot \cos\theta \cdot \hat{i} - R \cdot \sin\theta \cdot \hat{j} \tag{8}$$

and the magnitude becomes:

$$r = |\vec{r}| = \sqrt{\left(\frac{z}{\cos\beta}\right)^2 + \left(-R \cdot \cos\theta\right)^2 + \left(-R \cdot \sin\theta\right)^2} = \sqrt{R^2 + \frac{z^2}{\cos^2\beta}} \tag{9}$$

If the $\vec{r}$ is the vector position, then it must have a magnitude and a versor:

$$\vec{r} = r \cdot \hat{r} \tag{10}$$

In this case, the versor must be known:

$$\hat{r} = \frac{\vec{r}}{r} \tag{11}$$

The Biot-Savart law states that the field direction is given by the vector product between the carrying element and the versor of the Euclidian distance [5]:

$$d\vec{S} \times \hat{r} = d\vec{S} \times \frac{\vec{r}}{r} \tag{12}$$

$$\begin{aligned} d\vec{S} \times \hat{r} = &\left[\left(-R \cdot \sin\theta \cdot d\theta\right) \cdot \hat{i} + \left(R \cdot \cos\theta \cdot d\theta\right) \cdot \hat{j}\right] \times \\ &\times \left[\left(-R \cdot \cos\theta \cdot d\theta\right) \cdot \hat{i} + \left(-R \cdot \sin\theta \cdot d\theta\right) \cdot \hat{j} + \frac{z}{\cos\beta} \cdot \hat{k}\right] \end{aligned} \tag{13}$$

After matrix product of vectors it becomes:

$$d\vec{S} \times \hat{r} = R \cdot \left(\cos\theta \cdot \frac{z}{\cos\beta} \cdot \hat{i} + \sin\theta \cdot \frac{z}{\cos\beta} \cdot \hat{j} + R \cdot \hat{k}\right) \cdot d\theta \tag{14}$$

Heaving all the components, their values must be replaced in the basic formula to find out the contribution of a single length element for the magnetic field [2]:

$$d\vec{B} = \frac{\mu_0}{4\pi} \cdot \frac{I \cdot d\vec{S} \times \hat{r}}{r^2} = \frac{\mu_0 \cdot I}{4\pi \cdot r^2} \cdot \frac{d\vec{S} \times \vec{r}}{r} = \\ = \frac{\mu_0 \cdot I \cdot R}{4\pi \cdot (R^2 + z^2)^{3/2}} \cdot \left( \cos\theta \cdot \frac{z}{\cos\beta} \cdot \hat{i} + \sin\theta \cdot \frac{z}{\cos\beta} \cdot \hat{j} + R \cdot \hat{k} \right) \cdot d\theta \tag{15}$$

## 3. RESULTS

From the expression of the field $d\vec{B}$, the contributions from the *xOyOz* axis represented by the three versors $\hat{i}, \hat{j}, \hat{k}$ can be observed.

To find the contribution of the current element on all the length of the circle, the field expression must be integrated over the length in relation to the angle of rotation.

$$\vec{B} = \frac{\mu_0 \cdot I \cdot R}{4\pi \cdot (R^2 + z^2)^{3/2}} \cdot \int_0^{2\pi} \left( \cos\theta \cdot \frac{z}{\cos\beta} \cdot \hat{i} + \sin\theta \cdot \frac{z}{\cos\beta} \cdot \hat{j} + R \cdot \hat{k} \right) \cdot d\theta \tag{16}$$

After expanding this relation on separate axis components, it can bee seen the reason why the field has values only on transversal axis.

$$B_x = \frac{\mu_0 \cdot I \cdot R}{4\pi \cdot (R^2 + z^2)^{3/2}} \cdot \int_0^{2\pi} \cos\theta \cdot \frac{z}{\cos\beta} \cdot d\theta = \frac{\mu_0 \cdot I \cdot R}{4\pi \cdot r^3} \cdot \frac{z}{\cos\beta} \cdot \sin\theta \Big|_0^{2\pi} = 0 \tag{17}$$

$$B_y = \frac{\mu_0 \cdot I \cdot R}{4\pi \cdot (R^2 + z^2)^{3/2}} \cdot \int_0^{2\pi} \sin\theta \cdot \frac{z}{\cos\beta} \cdot d\theta = -\frac{\mu_0 \cdot I \cdot R}{4\pi \cdot r^3} \cdot \frac{z}{\cos\beta} \cdot \cos \Big|_0^{2\pi} = 0 \tag{18}$$

$$B_z = \frac{\mu_0 \cdot I \cdot R}{4\pi \cdot (R^2 + z^2)^{3/2}} \cdot \int_0^{2\pi} R \cdot d\theta = \frac{\mu_0 \cdot I \cdot R^2}{4\pi \cdot r^3} \cdot \theta \Big|_0^{2\pi} = \frac{\mu_0 \cdot I \cdot R^2}{2 \cdot \left( R^2 + \frac{z^2}{\cos^2 \beta} \right)^{\frac{3}{2}}} \tag{19}$$

## 4. CONCLUSIONS

It is clear that the magnetic field is null on the *Ox* and *Oy* axis because of the dependence on the angle $\theta$. The only component that has value, $B_z$, has also a very important property: it's value decreases exponential in relation to Euclidian distance at the point of measure.

If the point of measure is not on the central axis of the loop, the magnitude of the field is measured on the correspondent axis, *Oz*. In this case, the *cosβ* that appears increases the Euclidian distance, which causes a substantial drop of field.

Another important aspect is that, if the angle between $\vec{r}$ and $\vec{r'}$ reaches π/2 radians (the point of measure is perpendicular to the wire, not on the center of circle) the field value drops to 0:

$$d\vec{B} = \cos\alpha \cdot d\vec{B_z} \tag{20}$$

As closer the point of measure is to the center of the loop, the value of the field increases and gets the maximum potential at *z=0*.

All expressions presented help develop a better understanding of what happens with the magnetic field outside any encircled areas and the dependence on the angles of vector orientation.

## *REFERENCES*


[1] J. D. Jackson, *Classical Electrodynamics (3rd ed.)*, Wiley, New York, 1999.

[2] W. Lewin, J. Belcher and P. Dourmashkin. *8.02SC Physics II: Electricity and Magnetism, Fall 2010*. (MIT Open Course Ware: Massachusetts Institute of Technology), http://ocw.mit.edu/courses/physics/8-02sc-physics-ii-electricity-and-magnetism-fall-2010.

[3] V. Bălan, *Algebră liniară, geometrie analitică*, Editura Fair Partners, București,1999.

[4] M. Olteanu, *Analiza Matematică - noțiuni teoretice și probleme rezolvate*, Ed. Printech, București, 2005.

[5] J. C. Maxwell, *On Physical Line of Force,* Philosophical Magazine and Journal of Science, March 1861.

# INSTRUCTIONS FOR AUTHORS

Name **SURNAME**[1], Name **SURNAME**[2], **...**

[1] *Affiliation of 1st author,* [2] *Affiliation of 2nd author, ...*

*Email of 1st author, Email of 2nd author, ...(it is compulsory only for the first author)*

**Keywords: List 3-4 keywords** *(aligned to the left, 10 pt. bold, separated by commas; please choose keywords from IEEE Approved Indexing Keyword List)*

**Abstract***: Abstract of max. 200 words, justify, 10 pt. italic.*

## 1. INTRODUCTION

The paper must be written in English. It shall contain at least the following chapters: introduction, research course (mathematical algorithm); method used; results and conclusions, references.

### 1.1. Fonts

Use DIN A4 Format (297 x 210 mm) MSWord format. Margins: top, bottom, left and right 2.5 mm each. The text should be written on one side of the page only. Use Times New Roman fonts, line spacing 1.3. The font formats are: paper title: 14 pt, bold, italic, capital letters, author's name(s): 12 pt, regular for name and 12 pt., bold, for surname; Affiliation: 11 pt., italic; key words: 10 pt., bold; Abstract: 10 pt., italic, word Abstract in 10 pt., bold; chapter titles (do not use automatic numbering): 12 pt., bold, capital letters; subtitles: 12 pt., bold, lower case letters; subsubtitles: 12 pt., italic, lower case letters; body text: 12 pt., regular; tables and figures caption: 11 pt.; italic; references: author 11 pt.; regular, title 11 pt. italic, year, pages, ... in regular.

#### *1.1.1. Number of pages*

The number of pages is not restricted.

## 2. FIGURES AND TABLES

Figures have to be made in high quality, which is suitable for reproduction and printing. Don't include photos or color prints if there are not clearly intelligible in gray scale option. Place figures and tables at the top or bottom of a page wherever possible, as close as possible to the first reference to them in the paper. Use either *fig. 1* or *figure 1* when necessarily.

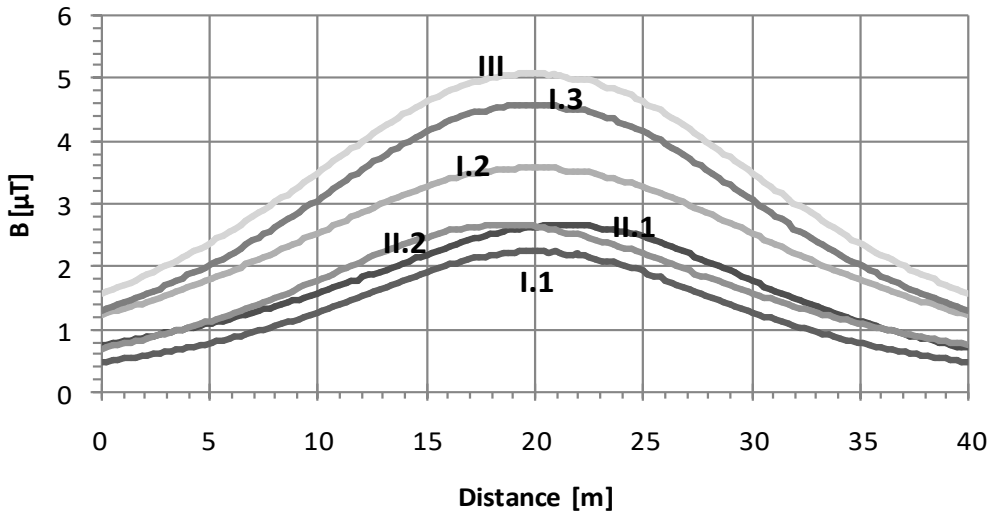


*Fig. 1. Magnetic flux density at 1 m above the ground*

Table 1. Transposing principle

| | *Circuit* | | | | | | | | | | | |
|---|---|---|---|---|---|---|---|---|---|---|---|---|
| | *1* | *2* | *1* | *2* | *1* | *2* | *1* | *2* | *1* | *2* | ***1*** | ***2*** |
| *1/3* | *R* | *T* | ***R*** | ***R*** | *R* | *S* | *R* | *T* | *R* | *S* | ***R*** | ***R*** |
| *line* | ***S*** | ***S*** | *S* | *T* | *S* | *R* | *S* | *R* | *S* | *T* | ***S*** | ***S*** |
| *length* | *T* | *R* | *T* | *S* | ***T*** | ***T*** | *T* | *S* | *T* | *R* | ***T*** | ***T*** |
| *1/3* | *T* | *S* | ***T*** | ***T*** | *T* | *R* | *T* | *S* | *T* | *R* | ***T*** | ***T*** |
| *line* | ***R*** | ***R*** | *R* | *S* | *R* | *T* | *R* | *T* | *R* | *S* | ***R*** | ***R*** |
| *length* | *S* | *T* | *S* | *R* | ***S*** | ***S*** | *S* | *R* | *S* | *T* | ***S*** | ***S*** |
| *1/3* | *S* | *R* | ***S*** | ***S*** | *S* | *T* | *S* | *R* | *S* | *T* | ***S*** | ***S*** |
| *line* | ***T*** | ***T*** | *T* | *S* | *T* | *S* | *T* | *S* | *T* | *R* | ***T*** | ***T*** |
| *length* | *R* | *S* | *R* | *T* | ***R*** | ***R*** | *R* | *T* | *R* | *S* | ***R*** | ***R*** |
| *Name* | ***I.1*** | | ***I.2*** | | ***I.3*** | | ***II.1*** | | ***II.2*** | | ***III*** | |

## 3. EQUATIONS

Equations are centred on page and are numbered in round parentheses, flush to right margin.

$$a = b + c \tag{1}$$

Between equations, not interfered by text, there is only one empty line:

$$a = b + c \tag{2}$$

$$a = b + c \tag{3}$$

In text respect the following rules: all variables are italic, constants are regular; the references are cited in the text between right parentheses [1], the list of references has to be arranged in order of citation.

*REFERENCES*

[1] International Commission on Non-ionizing Radiation Protection, *Guidelines for limiting exposure to time-varying electric, magnetic and electromagnetic fields (Up to 300 GHz)*, Health Physics, vol. 74, no. 1, pp. 494-522, 1998.

[2] A. Marincu, M. Greconici, *The electromagnetic field around a high voltage 110 KV electrical overhead lines and the influence on the biological systems*, Proceedings of the 5th International Power Systems Conference, pp. 357-362, Timisoara, 2003.

[3] Gh. Hortopan, *Compatibilitate electromagnetică*, Ed. Tehnică, 2005.